

Growing Massive Black Holes in a Local Group Environment: the Central Supermassive, Slowly Sinking, and Ejected Populations

Miroslav Micic^{1*}, Kelly Holley-Bockelmann^{2,3}, Steinn Sigurdsson⁴

¹ *Sydney Institute for Astronomy, School of Physics, The University of Sydney*

² *Department of Physics & Astronomy, Vanderbilt University*

³ *Department of Physics, Fisk University*

⁴ *Department of Astronomy & Astrophysics, Pennsylvania State University*

7 November 2021

ABSTRACT

We explore the growth of $\leq 10^7 M_\odot$ black holes that reside at the centers of spiral and field dwarf galaxies in a Local Group type of environment. We use merger trees from a cosmological N-body simulation known as Via Lactea II (VL-2) as a framework to test two merger-driven semi-analytic recipes for black hole growth that include dynamical friction, tidal stripping, and gravitational wave recoil in over 20,000 merger tree realizations. First, we apply a Fundamental Plane limited (FPL) model to the growth of Sgr A*, which drives the central black hole to a maximum mass limited by the Black Hole Fundamental Plane after every merger. Next, we present a new model that allows for low-level Prolonged Gas Accretion (PGA) during the merger. We find that both models can generate a Sgr A* mass black hole. We predict a population of massive black holes in local field dwarf galaxies – if the VL-2 simulation is representative of the growth of the Local Group, we predict up to 35 massive black holes ($\leq 10^6 M_\odot$) in Local Group field dwarfs. We also predict that hundreds of $\leq 10^5 M_\odot$ black holes fail to merge, and instead populate the Milky Way halo, with the most massive of them at roughly the virial radius. In addition, we find that there may be hundreds of massive black holes ejected from their hosts into the nearby intergalactic medium due to gravitational wave recoil. We discuss how the black hole population in the Local Group field dwarfs may help to constrain the growth mechanism for Sgr A*.

Key words:

Local Group, AGN feedback, supermassive black holes, dark matter halos, gravitational recoil, n-body simulations

1 INTRODUCTION

Supermassive black holes, with masses of $10^6 M_\odot \leq M \leq 10^{10} M_\odot$, are widely believed to dwell at the centers of elliptical galaxies and spiral bulges (e.g. Kormendy & Richstone 1995); the best known example is observed at the center of the Milky Way, with a mass

$M_{\text{SMBH}} = 4.2 \times 10^6 M_\odot$ (Ghez et al. 2008). There is abundant evidence that when a SMBH is in place, it transforms the structure and evolution of the galaxy, from powering active galactic nuclei at high redshifts (Greenstein & Matthews 1963, Rees 1984, Alexander et al. 2005, Fan 2005), to regulating star formation throughout the galaxy (Di Matteo et al. 2005, Croton et al. 2006, Cox et al. 2008), to scouring the galactic nucleus of stars during SMBH mergers (Ebisuzaki et

* E-mail: m.micic@physics.usyd.edu.au

al. 1991, Quinlan 1996, Makino 1997, Milosavljevic & Merritt 2001, Volonteri et al. 2003).

This deep connection between the evolution of SMBHs and galaxies is perhaps best encapsulated in a remarkable correlation between the SMBH mass and the velocity dispersion of the host spheroid (Gebhardt et al. 2000, Ferrarese & Merritt 2000, Tremaine et al. 2002, Marconi & Hunt 2003, Hopkins et al. 2007). The dispersion in the *black hole fundamental plane* (Hopkins et al. 2007) points to an intrinsically tight correlation, at least for a sample of nearby bright spiral and elliptical galaxies with clear dynamical SMBH signatures. However, on a smaller mass scale, in systems that have a mass comparable to the Milky Way mass or smaller, central SMBHs may become less common as bulges become less common (Ferrarese et al. 2006), and in some instances they disappear entirely, such as in the case of M33 (Merritt et al. 2001, Gebhardt et al. 2001), and NGC 205 (Valluri et al. 2005). Many of these bulgeless stellar systems host a nuclear star cluster instead. Nuclear star clusters are found in late-type spirals (Boker et al. 2002), and dwarf elliptical galaxies (Cote et al. 2006). This changeover may be the result of a competition between the SMBH and nuclear star cluster for the same gas reservoir. Nayakshin et al. (2009) shows that in massive galaxies with a spheroid velocity dispersion of $\sigma \geq 150 \text{ km s}^{-1}$, gas accretion onto the black hole dominates and a SMBH forms, while in galaxies with lower velocity dispersions, star formation generates a nuclear cluster. Note that such a star cluster does not exclude presence of an underweight SMBH (Nayakshin et al. 2009).

Several observational and theoretical studies have linked the SMBH mass to the mass of the host dark matter halo (Ferrarese 2002, Baes et al. 2003, Shankar et al. 2006). This relation is a boon to theorists because many of the leading explanations of SMBH birth and growth are driven by hierarchical structure formation (Hopkins et al. 2005, Wyithe & Loeb 2005, Granato et al. 2001, Menou et al. 2001, Adams et al. 2001, Monaco et al. 2000, Silk & Rees 1998, Haehnelt et al. 1998, Haehnelt & Kauffmann 2000, Cattaneo et al. 1999, Loeb & Rasio 1994), and are therefore tied to the mass of the dark matter halo.

In the current picture of SMBH assembly, the black hole begins life as a low mass “seed” black hole at high redshift. It’s not clear, though, when exactly these BH seeds emerge or what mass they have at birth. SMBH seeds may have been spawned from the accretion of low angular momentum gas in a dark matter halo (Koushiappas et al. 2004, Bromm & Loeb 2003, 2004), the coalescence of many seed black holes within a halo (Begelman & Rees 1978, Islam et al. 2004), or from an IMBH formed, perhaps, by runaway stellar collisions (Portegies Zwart et al. 2004, Miller & Colbert 2004, van der Marel 2004) or they could even be primordial (Mack et al. 2007). However, the most likely candidates for SMBH seeds are the remnants that form from the first generation of stars sit-

ting deep within dark matter halos (Madau & Rees 2001, Heger et al. 2003, Volonteri et al. 2003, Islam et al. 2003, Wise & Abel 2005) – so called Population III stars. With masses less than roughly $10^3 M_{\odot}$, these relic seeds are predicted to lie near the centers of dark matter halos at high redshifts (Bromm et al. 1999, Abel et al. 2000, 2002). Structure formation dictates that dark matter halos form in the early universe and hierarchically merge into larger bound objects, so naturally as dark matter halos merge, seed black holes sink to the center through dynamical friction and eventually coalesce.

Gas accretion is thought to play a critical role in fueling the early stages of black hole growth (David et al. 1987, Kauffmann & Haehnelt 2000, Merloni 2004), and this may explain the tightness of the $M_{\text{BH}} - \sigma$ relation (Burkert & Silk 2001, Haehnelt & Kauffmann 2000, Di Matteo et al. 2005, Kazantzidis et al. 2005, Robertson et al. 2006). Since high redshift galaxies are thought to be especially gas-rich, each merger brings a fresh supply of gas to the center of the galaxy, and new fuel to the growing supermassive black hole (Mihos & Hernquist 1994, Di Matteo et al. 2003). From a combination of gas accretion and binary black hole coalescence, it is thought that these Pop III-generated seeds may form the SMBHs we observe today (Soltan 1982, Schneider et al. 2002).

During a galaxy merger, each black hole sinks to the center of the new galaxy potential due to dynamical friction and eventually becomes bound as a binary (Kazantzidis et al. 2005; Escala et al. 2005). Dynamical friction then continues to shrink the orbit until the binary is hard (i.e. the separation between each black hole, a_{BBH} , is such that the system tends to lose energy during stellar encounters) (Heggie et al. 2007). Thereafter, further decay is mediated by 3-body scattering with the ambient stellar background until the binary becomes so close that the orbit can lose energy via gravitational radiation. In studies of static, spherical potentials, it may be difficult for stellar encounters alone to cause the binary to transition between the 3-body scattering phase and the gravitational radiation regime (Milosavljevic & Merritt 2003). However, in gas-rich or non-spherical systems, the binary rapidly hardens and coalesces into one black hole, emitting copious gravitational radiation in the process (Mayer et al. 2007, Kazantzidis et al. 2005, Berczik et al. 2006, Sigurdsson 2003, Holley-Bockelmann & Sigurdsson 2006).

Unless the black hole binaries stall at the final parsec, the longest timescale governing the coalescence of two black holes occurs when the host galaxies themselves are still merging. Here, the dynamical evolution of two merging galaxies is driven by the combined effect of *dynamical friction*, which brings the less massive galaxy, or satellite, to the center of the larger halo, or primary, and *tidal interaction* which strips mass from the satellite and further delays the merger (e.g. Richstone 1976, Aguilar & White 1986, Holley-

Bockelmann & Richstone 1999, Taffoni et al. 2003). If the dynamical friction timescale is longer than a Hubble time, the black holes carried by their host galaxies will not sink close enough to form a binary.

Sijacki et al. 2007 and Di Matteo et al. 2008 have performed state-of-the-art high resolution hydrodynamic simulations of cosmological structure formation, following the growth of high mass SMBHs at the centers of massive elliptical galaxies and clusters of galaxies. Their research was followed by similar semi-analytic work that incorporates a full treatment of dark matter dynamics, radiative gas cooling, star formation and energy feedback processes (Somerville et al. 2008). In this very elegant approach, the SMBH accretes gas through a *quasar mode* – nearly Eddington rate accretion following a galaxy merger (Croton et al. 2006) – and a *radio mode* – Bondi-Hoyle accretion associated with relativistic jets (Somerville et al. 2008). Both modes produce feedback that heats the surrounding gas. In this model, the feedback stops the accretion and locks the growth of the SMBHs to the fundamental plane. At the same time, the feedback also quenches the star formation, which explains the observed shallow metallicity, stellar density and entropy profiles. However, it has recently been suggested that the implementation and importance of AGN feedback may need to be reexamined (Ostriker et al. 2010). Also, radiation fields and winds produced by massive stars may provide the dominant feedback (Hopkins et al. 2010). In fact, it is worth mentioning that AGN feedback is just one of many feedback processes occurring in galaxy centers; supernovae, star formation, and galaxy mergers produce feedback as well (Sinha & Holley-Bockelmann 2010). It is not clear which feedback process contributes the most to the evolution of a given galaxy.

As well-developed as the current effort to understand SMBH growth is, most work has focused on growing the most massive SMBHs, found predominantly in dense environments. In a Local Group environment though, the galaxy morphology, dynamics, and star formation history are all dramatically different. Smaller stellar systems such as disk and dwarf galaxies, have SMBHs with lower masses ($\leq 10^6 M_\odot$) or no SMBHs at all for bulgeless galaxies like M33. In cosmological simulations, AGN feedback models create significant uncertainties for black hole growth in these lower mass halos (Booth & Schaye 2009). In addition, SMBHs in the Local Group are currently subluminal, implying a different relationship with gas consumption, at least in the present epoch, than the more massive end of the SMBH mass spectrum. Nonetheless, mergers are still expected to provide a key mechanism to channel gas to the galactic center. While “cold mode” gas accretion (Keres et al. 2005, Dekel et al. 2009) can channel large amounts of cold gas ($\leq 10^4 K$) to the galactic disk, this gas may not fuel the SMBH. Indeed, high resolution N-body-SPH simulations of Milky Way formation show that most

of the gas that is accreted originates from major mergers; even during the “radio mode”, where the gas is accreted by a Bondi - Hoyle mechanism, the gas reservoir is stocked not from the cold mode, but from the major mergers the Milky Way finished billions of years ago (J. Bellovary, private communication). Hence, galaxy mergers appear to drive SMBH growth in a wide range of masses.

One problem that can preferentially plague low mass galaxies is gravitational wave recoil. Recent calculations of binary black hole mergers indicate that gravitational wave recoil can kick a newly merged black hole with a speed as large as $\sim 4000 \text{ km s}^{-1}$ (Herrmann et al. 2007, Gonzalez et al. 2007a, 2007b, Kopitz et al. 2007, Campanelli et al. 2007, Schnittman & Buonanno 2007). The magnitude of the gravitational wave recoil imparted during any given merger depends on the mass ratio of each black hole, the spin magnitude and orientation with respect to the binary orbital plane, as well as the eccentricity of the orbit (Campanelli et al. 2007, Schnittman & Buonanno 2007, Baker et al. 2007). While certain spin alignment mechanisms (Bogdanovic et al. 2007, Dotti et al. 2010) could allow massive galaxies to retain their SMBHs, even moderate kicks can eject a growing SMBH from dwarf or high redshift galaxies (Merritt et al. 2004, Micic et al. 2006, Volonteri 2007, Schnittman 2007, Sesana 2007, Volonteri et al. 2010). There is tentative observations that suggest that gravitational wave recoil can indeed eject a SMBH from its host (Komossa et al. 2008). Given the greater vulnerability to recoil, the questionable importance of AGN feedback, and lack of SMBH in some galaxies, one can argue that SMBH growth may be substantially different for these lightest SMBHs in Local Group type of environments.

In this paper we use Via Lactea 2 (VL-2) evolutionary tracks to begin with an N-body merger tree that mimics the assembly of the Milky Way halo (Diemand et al. 2007, 2008). Upon this numerical merger tree we paint semi-analytic recipes for the galaxy and black hole growth. We follow two different merger driven recipes. The first approach is inspired by recent semi-analytic and numerical work on black hole growth (Somerville et al. 2008, Croton et al. 2006, Hopkins et al. 2005, 2007). Here, SMBHs grow slowly through low-level Bondi-Hoyle gas accretion tempered by AGN feedback – the radio mode; this growth is punctuated by rapid Eddington gas accretion triggered by a major merger – the quasar mode. This approach has been used to explain SMBH growth in massive stellar systems but not the growth of massive black holes in the Local Group. Here, SMBH growth is limited by the black hole fundamental plane. Hence, hereafter we call this approach Fundamental Plane limited (FPL). In the second recipe, we introduce a model for prolonged black hole gas accretion physically motivated by galaxy dynamics. In this model, the subgrid physics (stellar and AGN feedback, as well as accretion disk microphysics) is bundled into one pa-

parameter for gas accretion efficiency that can be constrained by future small-scale, fully general relativistic magneto-hydrodynamic AGN simulations. With this approach, gas accretion onto the black hole is based on the dynamics of the galaxy merger – fast at high rate for major mergers and prolonged at low rate for more minor mergers. This model does not use the black hole fundamental plane or the $M - \sigma$ relation to limit black hole growth. During a minor merger, the accretion time scale is longer, but the accretion rate is lower, since less gas is driven toward the BH by a smaller global perturbation. For major mergers, the accretion rate increases, though in practice it never reaches the Eddington rate. We call this approach Prolonged Gas Accretion (PGA). In addition to gas accretion, black holes grow through mergers with other black holes too. In both recipes, we model SMBH growth from direct mergers including gravitational recoil. Since the recoil velocity is highly dependent on BH spin and orientation, we create $\sim 20,000$ merger trees to examine the combination of BH spin parameters that favors the $M - \sigma$ relation at redshift zero.

The key difference between FPL and PGA models is in the implementation of AGN feedback. In FPL, the black hole fundamental plane is used to calibrate AGN feedback. In PGA, we use AGN feedback to suppresses the efficiency of gas accretion, while calibration parameters come from detailed small scale simulations of galaxy merger remnants.

We describe our method in section 2 and introduce our black hole growth prescriptions. In section 3, we present results, focusing on the evolution of our Sgr A* analogue in the FPL and PGA models. In Section 4, we present predictions for the local population of massive black holes, rogue black holes in the Milky Way, and ejected black holes into the nearby intergalactic medium. We discuss the implications of our results and future work in section 5.

2 METHOD

2.1 VL-2 Dark Matter Halo Merger Tree

In this paper, we use publicly-available VL-2 evolutionary tracks (Diemand et al. 2007, 2008). VL-2 is the highest resolution cosmological N-body simulation of Milky Way formation and evolution, and evolves a Λ CDM universe with WMAP3 parameters ($\Omega_M=0.238$, $\Omega_\Lambda=0.762$, $\sigma_8=0.74$ and $h=0.7$). The high resolution region of VL-2 is embedded within a periodic box with a comoving length of 40 Mpc. The evolutionary tracks consist of the time evolution from $z=27.54$ to $z=0$ of $\sim 20,000$ dark matter halos identified at redshift $z=4.56$. Halos have masses as small as $\sim 10^5 M_\odot$.

In our hybrid method, we combine dark matter halo merger trees obtained from VL-2 evolutionary tracks with an analytical treatment of the physical processes that arise in the dynamics of galaxy and

black hole mergers. Our N-body approach stops with the creation of the halo merger tree. We seed dark matter halos with Population III black holes until $z=5$, following the work of Trenti & Stiavelli 2009 (Fig 1 in Trenti et al. 2009), and follow their merger history from redshift 27.54 to 0 by constructing numerical merger trees interpolating between the snapshots at $z \leq 15$. To define the structure of each dark matter halo within the N-body generated merger tree, we assume a Navarro, Frenk, & White (hereafter, NFW) density profile (Navarro, Frenk & White 1996). We set the parameters of a given NFW halo using the approach presented in Bullock et al. 2001, assuming the typical virial mass of a dark matter halo to be $M_{\text{typ}} = 1.5 \times 10^{13} M_\odot$ at redshift zero. Note that only halos that are seeded with black holes or merging with other halos are retained in our merger tree. For each merger, we tag the more massive halo as the primary, with mass M_p , and the less massive halo as the secondary or satellite halo with mass M_s . Note that the properties of low mass dark matter halos in the mass range of VL-2 ($10^5 M_\odot \leq M \leq 2 \times 10^{12} M_\odot$) have not been studied in detail at $z \geq 3$.

Note that VL-2 evolutionary tracks do not include any halos or subhalos that were not present at $z=4.56$. Some halos are completely disrupted in mergers prior to that time (no subhalo counterpart at $z=4.56$), and some halos form after $z=4.56$. These halos are small in mass and would have been cut out of the merger tree anyway since they are either too small to host the black hole seed or too small to have relevant amounts of cold gas for either black hole accretion or star formation. Note that VL-2 does not necessarily represent the actual merger histories of Milky Way or Local Group.

2.2 SMBH Growth Prescriptions

We test two fundamentally different models for SMBH growth: Fundamental Plane Limited (FPL) and Prolonged Gas Accretion (PGA). In FPL, gas accretion onto the black hole is controlled by AGN feedback in such way that the SMBH mass does not grow above the black hole fundamental plane at any time. In PGA, we bundle star formation and AGN feedback, as well as accretion disk microphysics together into gas accretion efficiency parameter; the mass is not restricted to lie on the black hole fundamental plane.

Our only guideline is the mass of Sgr A* observed today. Since the mass of the SMBH at the center of the Milky Way is well-constrained, we can identify which physical processes during the growth are most important for the final black hole mass and test their parameter space. The first of these parameters applies to both models: the black hole seed's initial mass function (BHMF). We test various BHMFs and various values for the minimum and maximum black hole seed mass. A second effect that is present in both models is gravitational wave recoil (see Section 2.4).

The third parameter is unique in each model. In the FPL model, the third parameter is the mass accreted during the “radio” or quiescent mode of the AGN duty cycle. The SMBH growth during this phase is usually approximated by Bondi-Hoyle gas accretion, though this is not strictly necessary. We test various values for average mass accretion rate during this radio mode. Since the Bondi-Hoyle mechanism is commonly used, we may occasionally address this quiescent part of SMBH growth as the Bondi-Hoyle phase, but our approach does not depend on the actual growth mechanism here. In the PGA model, the third parameter is the gas accretion efficiency. In our implementation this parameter contains information on how the microphysics acts to suppress accretion onto the black hole, such as SNe feedback, accretion disk physics, etc. We treat all of these processes as free parameters to study the observable consequences at $z=0$.

In all models, we adopt Gnedin (2000) and Kravtsov et al. (2004) initial cold gas fractions ($f_{\text{cg}} \sim 10^{-5}$ for $M_{\text{halo}} \sim 3 \times 10^8 M_{\odot}$; $f_{\text{cg}} \sim 10^{-2}$ for $M_{\text{halo}} \sim 4 \times 10^9 M_{\odot}$; $f_{\text{cg}} \sim 0.13$ for $M_{\text{halo}} \geq 1 \times 10^{11} M_{\odot}$) in high redshift galaxies for a reionization range of $10 \leq z \leq 11$. In this manner we follow the approach of Somerville et al. (2008) for creating the gas reservoirs used for star formation and gas accretion onto the black holes. We do not include further multi mode accretion in the merger tree (i.e. Keres et al. 2005).

2.2.1 Fundamental Plane Limited Model

In the first model, FPL, we use the approach adopted by Somerville et al. (2008), but focus only on those aspects that are important for SMBH growth. In FPL, the SMBH grows through mergers and gas accretion. Gas accretion is controlled by two modes of AGN feedback. The quasar or “bright” mode occurs after the host galaxy goes through a major merger; this causes the central black hole to accrete gas exponentially until it reaches the Eddington limit, and it continues accreting at Eddington limit until it reaches a mass specified by the black hole fundamental plane. By design, the black hole mass at the end of each merger is proportional to the stellar mass of the spheroid M_{sph} in the model:

$$\log(M_{\text{BH}}/M_{\text{sph}}) = -3.27 + 0.36 \operatorname{erf}[(f_{\text{gas}} - 0.4)/0.28], \quad (1)$$

where f_{gas} is the amount of cold gas available for accretion (Somerville et al. 2008). The quasar mode is replaced by a radio mode until the next major merger. During the radio mode, the black hole accretes gas at lower rates associated with radiatively inefficient Bondi-Hoyle accretion, such as what occurs in an advection dominated accretion flow model (Fender et al. 2004). The Bondi-Hoyle accretion rate controls the black hole mass during the longer quiescent phase between galaxy mergers. In the Milky Way today, the SMBH mass is $4.2 \times 10^6 M_{\odot}$ (Ghez et al. 2008), and the Bondi-Hoyle rate is $\sim 5 \times 10^{-5} M_{\odot} \text{yr}^{-1}$ (Quataert &

Gruzinov 2000, Melia & Falcke 2001). Since we know the current Sgr A* mass and the accretion rate observed today, we can determine how well the FPL model can match observations. To simplify our investigation we adopt an average Bondi-Hoyle accretion rate during the radio mode over a Hubble time. The Bondi-Hoyle accretion rate in our model is averaged over all radio mode phases the galaxy goes through and since it explicitly excludes AGN feedback which would blow away the gas, the Bondi-Hoyle accretion rate we use is a lower constraint. If we model AGN feedback, the derived accretion rates would be higher.

2.2.2 Prolonged Gas Accretion Model

The SMBH in our PGA model grows through a combination of black hole mergers and gas accretion, inspired by Micic et al. (2007). To review the approach, we assumed that major galaxy mergers would funnel gas to the black hole in each of the progenitors and activate an Eddington-limited growth phase for a Salpeter time. The black hole mass in Micic et al. (2007) grew as: $M_{\text{BH}}(t) = M_{\text{BH},0}(t_0) \exp(\Delta t/t_{\text{sal}})$, where $\Delta t = t - t_0$, $t_{\text{sal}} \equiv \epsilon M_{\text{BH}} c^2 / [(1 - \epsilon)L]$, ϵ is the radiative efficiency, L is the luminosity, and c is the speed of light; in this picture the black hole mass would roughly double in 40 Myr (Hu et al. 2006). We distinguished two cases depending on the mass ratio of merging dark matter halos. The first is a more conservative criterion that allows black holes to accrete gas if the mass ratio of the host dark matter halo is less than 4:1 – a major merger. The second case sets an upper constraint on the final black hole mass by allowing gas accretion as long as the merging dark matter halos have a mass ratio less than 10:1 – on the cusp of what is considered a minor merger. Since our black holes merged promptly after the halos merged, the accretion timescale and efficiency for major mergers was the same regardless of the mass ratio or redshift.

In this paper, we continue to model the black hole growth as one of extended gas accretion excited by major mergers. At high redshift, this is likely a good assumption, though note that at low redshift when mergers are infrequent, secular evolution such as bar instabilities may dominate the gas (and therefore black hole) accretion. Integrated over the whole of a black hole lifetime, though, this major merger-driven gas accretion is likely to be the dominant source of gas inflow. Since the black hole growth is so strongly dependent on what fuel is driven to the center during galaxy mergers, it is important to characterize this merger-driven mass growth, including the critical gas physics that may inhibit or strengthen this nuclear supply. We are motivated by numerical simulations that include radiative gas cooling, star formation, and stellar feedback to study the starburst efficiency for unequal mass ratio galaxy mergers (Cox et al. 2008), which finds that the gas inflow depends strongly on the mass ratio of the galaxy (see also, e.g., Hernquist 1989,

Mihos & Hernquist 1994). This study parametrizes the efficiency of nuclear star formation (i.e. gas supply and inflow), α , as a function of galaxy mass ratio. In a broader sense, this study shows how much gas is available for either star formation or gas accretion onto the central black hole. These two processes compete for the same gas and the outcome (nuclear cluster versus SMBH) depends on the mass of the host spheroid (Nayakshin et al. 2009). The efficiency of gas inflow is described by:

$$\alpha = \alpha_{\text{slope}} \left(\frac{M_s}{M_p} - \alpha_0 \right)^{0.5}, \quad (2)$$

where α_0 defines the mass ratio below which there is no enhancement of nuclear star formation (i.e. gas inflow), and α_{slope} is the fitted slope of the solid line in Cox et al. (2008), Fig 15. Here, the gas accretion efficiency has a maximum of 0.56 for 1:1 halo mergers with $\alpha_{\text{slope}}=0.6$, and falls to zero at α_0 . This parametrization is insensitive to the stellar feedback prescription. We use α to define how efficiently the merger funnels the galaxy's gas to the black hole accretion disk. In general, all feedback processes (stellar or black hole) can be contained in α_{slope} . Only small scale numerical simulations of gas accretion in AGNs, with fully implemented and resolved gas physics can relate α_{slope} to the mass ratio of merging galaxies. In Cox et al. (2008), the fitted α_0 parameter suggests gas inflow is sharply curtailed for mass ratios larger than 9. We set the cut off mass ratio to $M_p/M_s = 10$ in order to compare with our previous black hole growth prescription (Micic et al. 2007). We adopt $\alpha_{\text{slope}} = 0.6$ as in Cox et al. (2008).

Now that we have implemented a realistic description of the merger time for each black hole within a halo (see next section), we allow them to grow for a physically-motivated accretion timescale. The accretion of gas onto both the incoming and central black hole starts when the two black holes are still widely separated, at the moment of the first pericenter passage, and continues until the black holes merge (c.f. Di Matteo et al. 2005, Colpi et al. 2007). This sets the accretion timescale, t_{acc} , as follows: $t_{\text{acc}} = t_{\text{df}}(r=r_{\text{vir}}) - t_{\text{dyn}}(r=r_{\text{vir}})$, where $t_{\text{df}}(r=r_{\text{vir}})$ is the merger timescale including dynamical friction, and $t_{\text{dyn}}(r=r_{\text{vir}})$ is dynamical time at virial radius r_{vir} , which marks the first pericenter pass of the black hole. By stopping the accretion as the black holes merge, we roughly model the effect of black hole feedback in stopping further accretion.

Putting these pieces together, the mass accreted by a black hole during $t_{\text{acc}}(r=r_{\text{vir}})$ is:

$$M_{\text{acc}} = M_{\text{BH},0} (e^{\frac{\alpha t_{\text{acc}}}{t_{\text{sal}}}} - 1), \quad (3)$$

where $M_{\text{BH},0}$ is the initial black hole mass, α is the starburst efficiency (Cox et al. 2008), and t_{sal} is defined above. After t_{df} , the incoming black hole merges with the SMBH at the center and a new SMBH is

formed after having accreted gas for t_{acc} . The accretion time and efficiency both implicitly encode the large-scale dynamics of the merger and the bulk gas accretion into the nuclear region, while t_{sal} describes the accretion disk physics. As before, we set the Salpeter accretion efficiency to 0.1 (Shakura & Syunyaev 1973).

2.3 Dynamical Friction

Dynamical friction allows massive black hole binaries to form at the center of a galaxy in two ways. First, dynamical friction expedites the merger of two dark matter halos and later the merger of the galaxies they host. In this manner, merging galaxies can efficiently shepherd massive black holes to the center of the new system, roughly to the inner kiloparsec (see Colpi et al. 2007 for a review). Second, dynamical friction from the gas in the disk carries black holes deeper toward the galactic center, where they form binary and eventually merge (e.g. Begelman, Blandford & Rees 1980, Escala et al. 2005, Kazantzidis et al. 2005, Dotti et al. 2007). We model both effects as follows:

The time for a satellite to sink to the center of a primary can be approximated using Chandrasekhar dynamical friction (Binney & Tremaine 1987):

$$t_{\text{chandra}} = \frac{1.17}{\ln \Lambda} \frac{r_{\text{circ}}^2 v_c \epsilon^\alpha}{GM_s}, \quad (4)$$

where $\ln \Lambda$ is the Coulomb logarithm, $\ln \Lambda \approx \ln(1 + M_p/M_s)$. To define the satellite orbit, we adopt values suggested by numerical investigations (Colpi et al. 1999) and used in previous semi-analytical work (Volonteri et al. 2003): the circularity $\epsilon^\alpha = 0.8$, and the circular velocity v_c is determined at $r_{\text{circ}} = 0.6 r_{\text{vir}}$. For a $10^{12} M_\odot$ halo, $r_{\text{vir}} \sim 300$ kpc.

Assuming that each merging galaxy carries a massive black hole at its center, t_{fric} is the merging time for massive black holes when all other processes (3-body scattering, gas dynamical friction, gravitational radiation, etc.) involved in the formation and later shrinking of the black hole binary are efficient and fast. Due to tidal stripping and possible resonant interactions, simulations have shown that the Chandrasekhar formula underestimates the merger time, especially in the case of minor mergers (e.g. Holley-Bockelmann & Richstone 1999, Weinberg 1989). If this is true, then semi-analytic studies of black hole merger rates using a Chandrasekhar formalism for the merger time will overestimate the true number of black hole mergers.

In an effort to better parametrize dynamical friction, Boylan-Kolchin et al. 2008 used N-body simulations to study dark matter halo merging timescales, and confirmed that the Chandrasekhar formalism does underestimate the merger time, by a factor of ≈ 1.7 for $M_p/M_s \approx 10$ and a factor of ~ 3.3 for $M_p/M_s \approx 100$. They propose a fitting formula that accurately predicts the timescale for a satellite to sink from the virial radius to the host halo center:

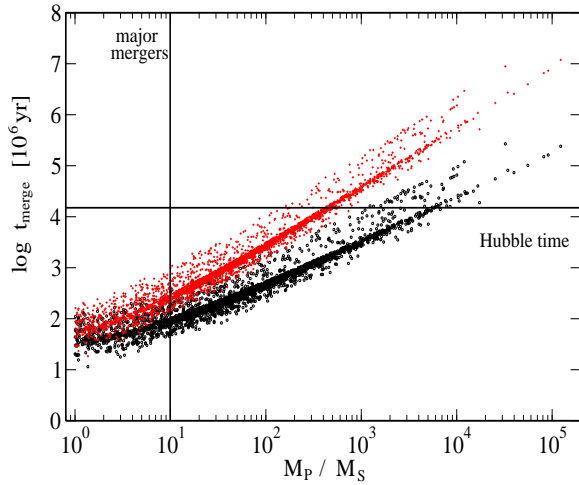


Figure 1. Time for each satellite to reach the primary halo center as a function of the mass ratio of merging halos. Black circles represent the Chandrasekhar dynamical friction time and red pluses represent the merging time calculated from a simulation-based numerical fit (Boylan-Kolchin 2008). Both timescales are compared to the Hubble time and mass ratios are compared to major mergers. Merging halos above the horizontal black line will not finish their merger and are removed from the merger tree, but their positions are updated within the primary halo.

$$\frac{\tau_{\text{merge}}}{\tau_{\text{dyn}}} = A \frac{(M_{\text{host}}/M_{\text{sat}})^b}{\ln(1 + M_{\text{host}}/M_{\text{sat}})} \exp \left[c \frac{j}{j_c(E)} \right] \left[\frac{r_c(E)}{r_{\text{vir}}} \right]^d, \quad (5)$$

where $b = 1.3$, $c = 1.9$, $d = 1$, $A = 0.216$, circularity $j/j_c(E) = 0.5$, $r_c(E)/r_{\text{vir}} = 0.65$, as defined in Boylan-Kolchin et al. 2008. The dynamical time, τ_{dyn} , is given at virial radius as:

$$\tau_{\text{dyn}} \equiv \frac{r_{\text{vir}}}{V_c(r_{\text{vir}})} = \left(\frac{r_{\text{vir}}^3}{GM_{\text{host}}} \right)^{1/2}, \quad (6)$$

where $V_c(r_{\text{vir}}) = (GM_{\text{vir}}/R)^{1/2}$.

Figure 1 shows the dark matter halo merger timescale for each pair of merging halos for both dynamical friction estimates. We have calculated the dark matter halo merger rate with both the Chandrasekhar dynamical friction formula and the Boylan-Kolchin numerical fit (Holley-Bockelmann et al. 2010). Unless otherwise stated, we adopt the Boylan-Kolchin timescale for all calculations.

It is expected that in gas-rich galaxies, dynamical friction from the gas would bring two black holes close enough to form a binary whose orbit would shrink efficiently, passing quickly from a binary in the 3-body scattering phase to one emitting significant gravitational radiation (Escala et al. 2005, Kazantzidis et al. 2005, Dotti et al. 2007). Numerical simulations indicate that two black holes will sink from ~ 1 kpc to form a binary with a separation of less than a parsec in ~ 10 Myrs. We incorporate this physics by calculating the dynamical friction timescale from the virial

radius to the inner kpc, and then assume that the two black holes merge 10 Myr afterward. In practice, the dynamical friction timescale from equations 1 and 2 from the inner kpc to the bound binary stage is often of order 10 Myr; the power of this gas-rich assumption lies in that it entirely circumvents the so-called ‘final-parsec’ problem thought to exist for low mass ratio mergers of $10^{6.5} M_{\odot} \leq M_{\text{BH}} \leq 10^8 M_{\odot}$ within static, spherical, gas-poor galaxy models (e.g. Milosavljevic & Merritt 2003). We explicitly assume that the black holes in our simulation do not stall at the final parsec before merger, and instead are ushered efficiently into the gravitational radiation stage where they coalesce; this assumption may hold even in the case of gas-poor galaxy models as long as the model is not spherical or in equilibrium (e.g. Holley-Bockelmann & Sigurdsson 2006, Berczik et al. 2006, R. Spurzem, private communication). Note that this implies that if we assume that each halo initially carries a black hole at its center, and that each host galaxy is gas-rich, figure 1 also estimates the time for a black hole to sink from the virial radius to the center of the host galaxy, become a bound black hole binary, and inspiral due to gravitational radiation.

In our initial work (Micic et al. 2007), mergers of dark matter halos trigger the immediate merger of the black holes they are hosting. In this paper, subsequent mergers of the central black holes are delayed to account for dynamical friction of the halos and the black holes within the galaxy. Black holes will not merge if their merger time is larger than a Hubble time, and in that case, we advance the black hole position within the primary halo at each timestep. Knowing the dynamical friction timescale for each merger, we postpone the black hole mergers accordingly. For the final kpc, we assume that ambient gas and/or non-sphericity will cause two black holes to coalesce within 10 Myrs.

2.4 Gravitational Recoil

Binary black holes strongly radiate linear momentum in the form of gravitational waves during the plunge phase of the inspiral – resulting in a “kick” to the new black hole. This, in itself, has long been predicted as a consequence of an asymmetry in the binary orbit or spin configuration. Previous kick velocity estimates, though, were either highly uncertain or suggested that the resulting gravitational wave recoil velocity was relatively small, astrophysically speaking. Now, recent results indicate the recoil can drive a gravitational wave kick velocity as fast as $\sim 4000 \text{ km s}^{-1}$ (Herrmann et al. 2007, Baker et al. 2007, Gonzalez et al. 2007a, 2007b, Koppitz et al. 2007, Campanelli et al. 2007, Schnittman & Buonanno 2007, Lehner & Moreschi 2007, McWilliams 2008, Lousto & Zlochower 2009, Sperhake 2009). In reality, much smaller values than this maximum may be expected in gas-rich galaxies due to the alignment of the orbital angular momentum

and the spins of both black holes (Bogdanovic et al. 2007).¹ Recent studies also hint at a potential purely general relativistic spin alignment mechanism (Kesden et al. 2010). However, even typical kick velocities ($\sim 200 \text{ km s}^{-1}$) are interestingly large when compared to the escape velocity of most astronomical systems – low mass galaxies, as an example, have an escape velocity of $\sim 200 \text{ km s}^{-1}$ (e.g. Holley-Bockelmann et al. 2007). The effect of large kicks combined with a low escape velocity from the centers of small dark matter halos at high redshift may play a major role in suppressing the growth of black hole seeds into SMBHs. Even the most massive dark matter halo at $z \geq 11$ can not retain a black hole that receives $\geq 150 \text{ km s}^{-1}$ kick (Merritt et al. 2004, Micic et al. 2006). We incorporate the effect of recoil velocity on the growth of the SMBH by assigning a kick to each black hole merger in our merger tree. We follow the approach adopted by Holley-Bockelmann et al. (2007), which uses the parametrized fit of Campanelli et al. 2007 to generalize the recoil velocity as a function of the mass ratio of the merging black holes, each individual black hole’s spin amplitude, and the alignment to the orbital angular momentum. We assume that as black holes form a hard binary, their orbits will be highly circular and the eccentricity is close to zero:

$$v_{\text{kick}} = [(v_m + v_{\perp} \cos \xi)^2 + (v_{\perp} \sin \xi)^2 + (v_{\parallel})^2]^{1/2}, \quad (7)$$

where

$$v_m = A \frac{q^2 (1-q)}{(1+q)^5} \left[1 + B \frac{q}{(1+q)^2} \right], \quad (8)$$

$$v_{\perp} = H \frac{q^2}{(1+q)^5} (\alpha_2^{\parallel} - q \alpha_1^{\parallel}), \quad (9)$$

and

$$v_{\parallel} = K \cos(\Theta - \Theta_0) \frac{q^2}{(1+q)^5} (\alpha_2^{\perp} - q \alpha_1^{\perp}). \quad (10)$$

Here, the fitting constants are $A = 1.2 \times 10^4 \text{ km s}^{-1}$, $B = -0.93$, $H = (7.3 \pm 0.3) \times 10^3 \text{ km s}^{-1}$, and $K \cos(\Theta - \Theta_0) = (6.0 \pm 0.1) \times 10^4$, while the subscripts 1 and 2 refer to the first and second BH respectively; \perp and \parallel stands for perpendicular and parallel to the orbital angular momentum; the mass ratio $q \equiv M_2/M_1$; the reduced spin parameter $\alpha_i \equiv S_i/M_i^2$, where S_i is the spin angular momentum of BH i . The orientation of the merger is specified by: Θ , the angle between the “in-plane” component of $\delta^i \equiv (M_1 + M_2) (S_2^i/M_2 - S_1^i/M_1)$ and the infall direction at merger; Θ_0 , the angle between δ^i and the initial direction of motion; and ξ , the angle between the unequal mass and spin contribution to the recoil in the orbital plane.

We assume that the orbit is circular, and we take the mass ratio of merging black holes directly from our

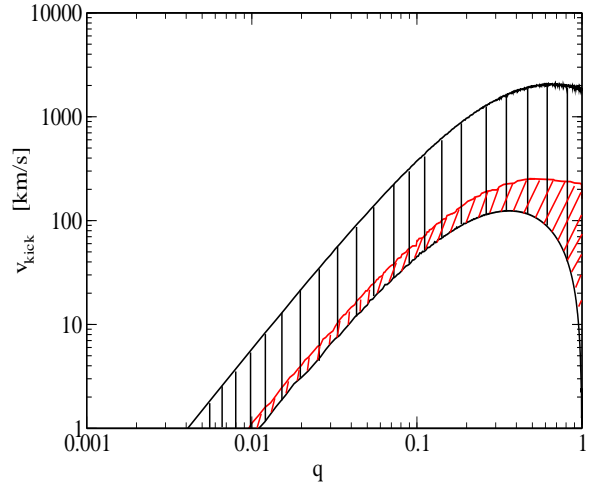


Figure 2. Distribution of gravitational recoil as a function of the mass ratio of merging black holes on circular orbits. The black lines represent random spin orientations and amplitudes – the K1 distribution. In red is the kick range when the spin orientation of the binary black holes aligns with the orbital momentum of the binary – the K2 distribution. If the kick is larger than the escape velocity, the black hole is ejected from the halo.

merger tree. We have the following free parameters: the spin amplitude and orientation of each black hole, and the orientation of the merger. We explore two spin distributions. The K1 model chooses the spin parameters from a uniform distribution, while the K2 model assumes the black hole spins are aligned with the orbital angular momentum (Bogdanovic et al. 2007). Figure 2 shows the distribution of kick velocities for both models. We apply both kick velocity distributions to the mergers in our merger tree using 1000 realizations each. This yields 2,000 Milky Way merger trees for the PGA model and 2,000 for the FPL model.

For each black hole merger, we calculate the kick velocity and compare it to the escape velocity of the host halo at the time of merger. If the kick is larger than the escape velocity, the resulting black hole is removed from the center of the host halo and from the merger tree. As the result, the host halo will not have a central black hole for a period of time. Subsequently, when the next black hole sinks to the center, it will simply take place of the central black hole. Depending on how often the central black hole is ejected, the final SMBH mass may be substantially smaller. The sequence and number of kicks in one merger tree realization depends on our kick distribution. Over many realizations, we can produce a probability function for the final black hole mass for each model.

¹ However, recent observations (Komossa et al. 2008) may show evidence for large kick velocities $\sim 2500 \text{ km s}^{-1}$.

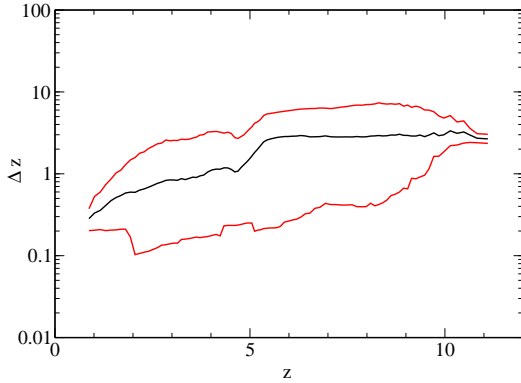


Figure 3. Thick black - the average change in the merger redshift when dynamical friction is applied as a function of merger redshift (excluding dynamical friction). Red lines represent the minimum and maximum shift in the black hole merger redshift. Dynamical friction postpones black hole mergers toward lower redshifts, making them louder LISA sources and increasing the local rate as well.

3 RESULTS

Black hole mergers postponed for longer than a Hubble time will not occur, which reduces the merger rate over all redshifts. Those mergers that are postponed but have a merging timescale less than a Hubble time will merge at lower redshifts. This is made explicit in figure 3, which plots the average change in redshift for a merger as a function of redshift if one includes dynamical friction. Black hole mergers at redshift 10 are, on average, pushed to redshift 7, for example. This results in an increase in the black hole merger rate at low redshifts. Since each merger occurs at a lower redshift, it will certainly be a louder gravitational wave source, and any associated electromagnetic signature will be brighter, as well (Holley-Bockelmann et al. 2010).

Interestingly, including dynamical friction from gas at distances smaller than 1 kpc does not make difference in our merger time scales. Those black holes that reach 1 kpc from the galactic center will reach a parsec even without the gas – gas is simply invoked to ensure that the black holes pass through the 3-body scattering stage efficiently. For the rest of this paper, we adopt the Boylan-Kolchin dynamical friction fit as a realistic treatment of the black hole merger timescale.

3.1 Realizations of Supermassive Black Hole Growth

Figure 4 shows the merger rates in our volume for those dark matter halos that merge in less than a Hubble time within the mass range $10^7 M_\odot \leq M_{\text{DMH}} \leq 10^{13} M_\odot$, for various mass ratios and combined masses of merging dark matter halos. In our volume, all the mergers that occur at redshifts $z \leq 1.5$ will not finish in less than a Hubble time, as these mergers are

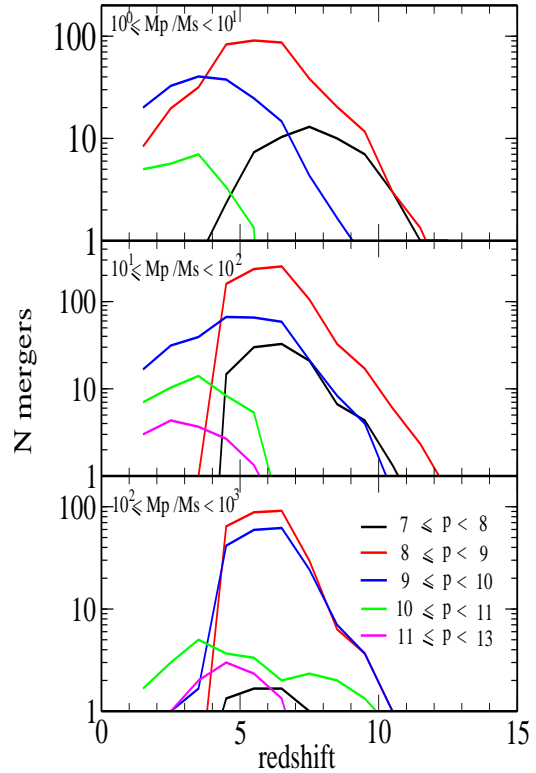


Figure 4. Dark matter halo merger rates as a function of redshift for all halos that finish merging by redshift zero. Three panels show various ranges for the halo mass ratio and the total combined halo mass. M_P is the primary halo mass, M_S is the satellite mass, and the total mass is defined by $p = \log(M_P + M_S)$. The panel with $M_P/M_S \leq 10$ shows merger rates for major mergers that activate gas accretion onto their black holes.

all high mass ratio. We remind the reader, though, that these halo merger rates are calculated for VL-2 40 Mpc³ simulation box. This model, by design, has no Galaxy Clusters, or even rich local groups, and it is for sparse local groups. The VL2 host halo was specifically chosen “not” to have undergone a major merger more recently than about $z \sim 1$. Almost all the low redshift mergers for this mass range SMBH are in richer, denser environments, which are just not covered in this model. A better global rate for these low mass halos will be achieved with more of these volumes.

Since in PGA the merger timescale is larger for higher mass ratio halos, the black hole gas accretion time scale is longer as well. Figure 5 shows this time scale for black holes hosted by dark matter halos that merge with mass ratio M_P/M_S and combined mass $p = \log(M_P + M_S)$. Notice that gas accretion is activated only for a small range of halo mass ratios $M_P/M_S \leq 10$ (the dashed line in figure 5). For these mergers, the black holes do not accrete for longer than ~ 1000 Myr, and the accretion efficiency is strongly damped as the

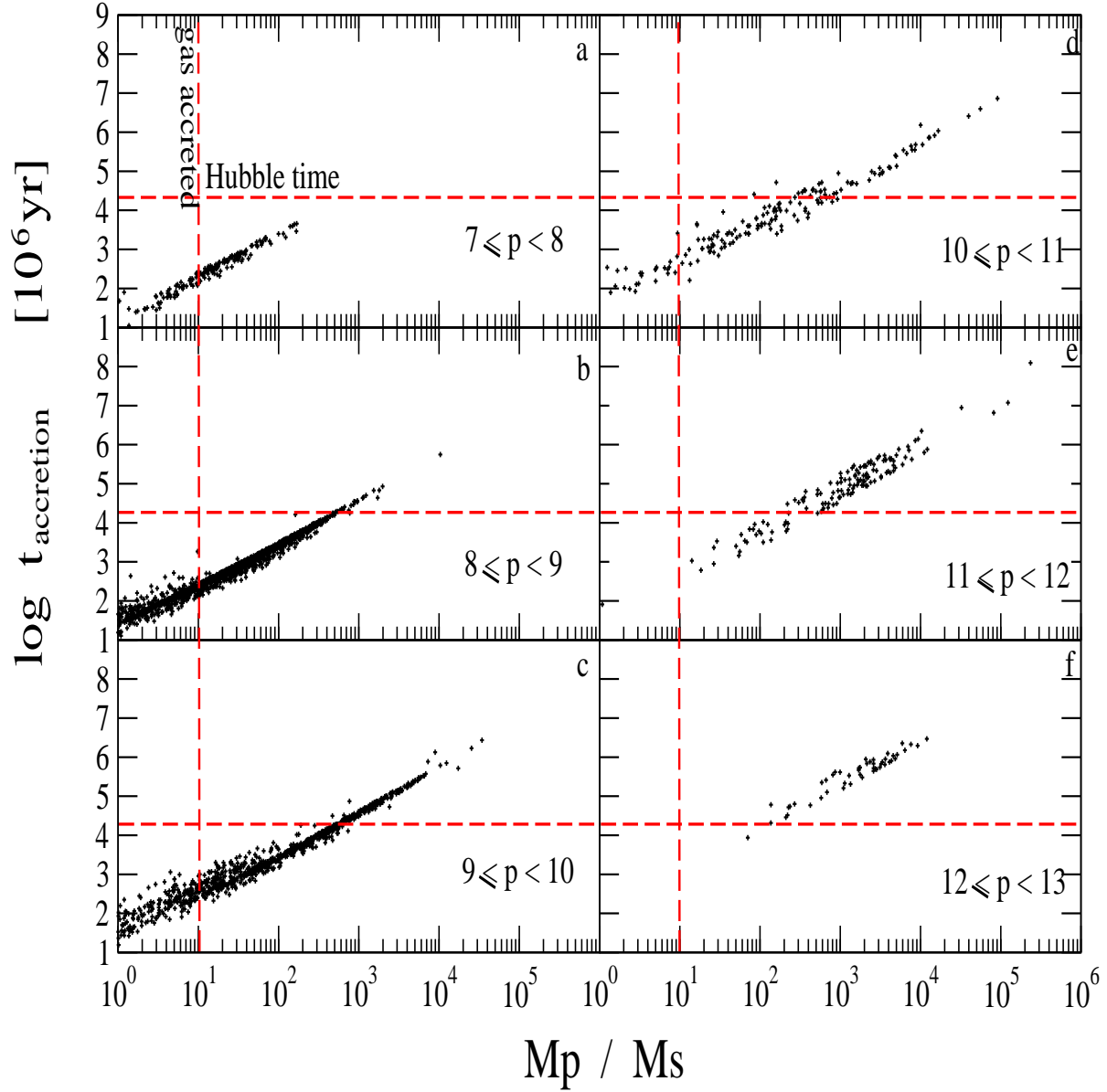


Figure 5. Gas accretion time, t_{acc} , for a central black hole in a satellite halo of mass M_{sat} that is merging with a primary halo of mass M_{prim} in the PGA model. The total mass is denoted by $p = \log(M_s + M_{\text{prim}})$, and $t_{\text{acc}} = t_{\text{merger}} - t_{\text{dyn}}$ where t_{merger} is the merger time scale, and t_{dyn} is the dynamical time, making accretion begin at the first pericenter pass. Halos that merge with mass ratios less than 10 (vertical line) will allow gas accretion onto the black holes. Only satellite halos with mass $\leq 10^{11} M_{\odot}$ will have an accreting central black hole.

halo mass ratio tends toward 10:1 – in no case does the system reach the Eddington limit.

Figure 5 offers valuable information about the FPL model as well. Panels e and f show that there are no mergers with mass ratios 10:1 or less for halos above $10^{11} M_{\odot}$. In fact, the halo that VL-2 marks as the Milky Way halo does not go through any major merg-

ers at low redshift. In the context of FPL, the quasar mode of rapid gas accretion occurs in Milky Way progenitors at high redshifts while the radio mode dominates most of the Sgr A* growth at low redshifts. We should also point out that VL-2 merger history of Milky Way is just one of the possible merger histories, and perhaps not the true one.

3.1.1 The Initial Mass Function of Black Hole Seeds.

Galaxies in the mass range of the VL-2 simulation have values for escape velocities comparable to the amplitudes of gravitational wave recoil for black hole mergers with mass ratios $q \geq 0.1$, even in the case of the lower K2 kick distribution. If we are to seed these galaxies with their first black holes, the choice of the black hole mass function (BHMF) will determine the mass ratio of merging black holes. We examine the influence of the choice of BHMF on VL2 merger trees in 1,000 kick realizations for BHMFs with constant values of 100; 1000; and 5000 M_\odot seeds; and also for random values in the mass ranges 10 - 200 M_\odot ; 10 - 500 M_\odot ; and 10 - 1,000 M_\odot . We find that having a constant BHMF or one in a narrow mass interval leads to close-to-equal mass ratio black hole mergers. These mergers have the highest gravitational wave recoil and ejects of black holes in high redshift dwarf galaxies, which suppresses SMBH growth. Due to the uncertainty in the formation channel for seed black holes, as well as the lack of theoretical constraints on primordial gas fragmentation during PopIII star formation (Glover et al. 2010), 10 - 1,000 M_\odot is the least biased of our BHMFs. We adopt this flat BHMF hereafter for the seeds in our merger trees in both the FPL and PGA models. Note that the seed mass in the FPL model is much less relevant than in the PGA model, because the black hole can not grow more massive than what is dictated by the black hole fundamental plane, regardless of the initial seed mass.

3.1.2 Massive Black Hole Accretion Properties

With the adopted flat BHMF, the only constraints in the FPL model are the time-average Bondi-Hoyle accretion rate during the radio mode and the strength of gravitational wave recoil. We start by running Milky Way merger trees for various values of the accretion rate and recoil distribution, looking for the values which, in combination with the accretion during quasar mode, produce a $\sim 4.2 \times 10^6 M_\odot$ black hole at $z=0$ in the majority of merger tree realizations. This condition is satisfied for the merger trees with $\dot{m}_{\text{bondi}} = 7 \times 10^{-4} M_\odot \text{yr}^{-1}$ (brown horizontal line in figure 6 up), consistent with the observations of accretion rates in low mass AGNs in the local Universe. It has been suggested that the Milky Way has evolved from a similar low mass AGN, which explains the fact that the observed value for accretion in Sgr A* today is an order of magnitude smaller than this best fit accretion rate. Outside of the Sgr A* analogue, there are also 35 field dwarf galaxies at $z=0$ with central black holes (see section 4.1). Figure 6 shows black hole accretion properties during the quasar and radio mode for the merger tree that excludes recoil, which corresponds to the maximum accretion. In this model, Milky Way progenitors go through their last quasar mode between $z=2$ and $z=3$ (upper panel, Fig 6), after which Bondi-

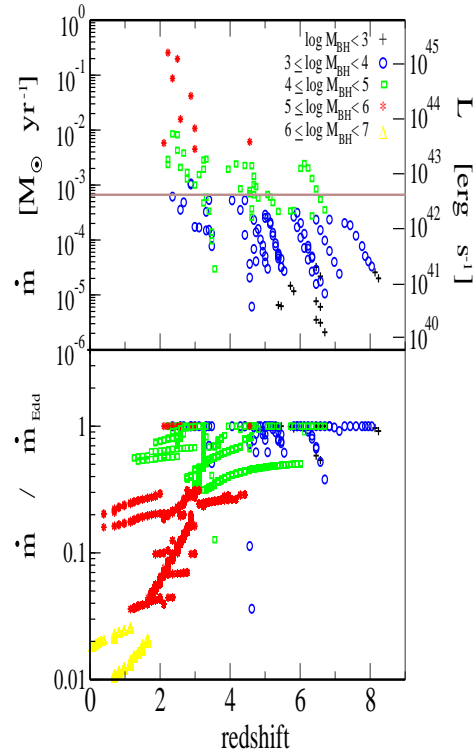


Figure 6. Accretion rates and luminosities during the quasar and radio modes for the FPL model (recoil excluded). The upper panel shows gas accretion rates and luminosities for all black holes during a random short time interval ($\delta t = t_f - t_i$). Points represent the quasar mode, while the brown horizontal line represents the radio mode. The black hole mass in the quasar mode increases at lower redshifts, with the final accretion episode between $z=3$ and $z=2$. Bondi - Hoyle accretion is the dominant growth mechanism at redshift $z \leq 2$. The bottom panel shows the gas accretion rate at short time intervals compared to the Eddington rate (quasar and radio modes combined). Most black holes accrete at the Eddington rate by design.

Hoyle accretion becomes the dominant mechanism of Sgr A* growth (horizontal line in upper panel, Fig 6). In the bottom panel of figure 6, the same accretion rate is compared to the Eddington rate. Most of the accretion occurs at the Eddington rate – this is expected since the assumption is built in that the black holes reach the Eddington rate very quickly. In many cases, however, accretion is not activated at all because the host galaxy is small and the spheroid mass prevents the growth of central black hole to match the black hole fundamental plane.

By excluding kicks, figure 7 shows the upper constraint on black hole accretion properties for all black holes in the PGA merger tree. Recall that the BHMF is flat and the accretion efficiency is set by simulations. With the choice of BHMF and gas inflow efficiency fixed in this model, kicks are the only free parameter. Black holes in the PGA model can grow beyond the

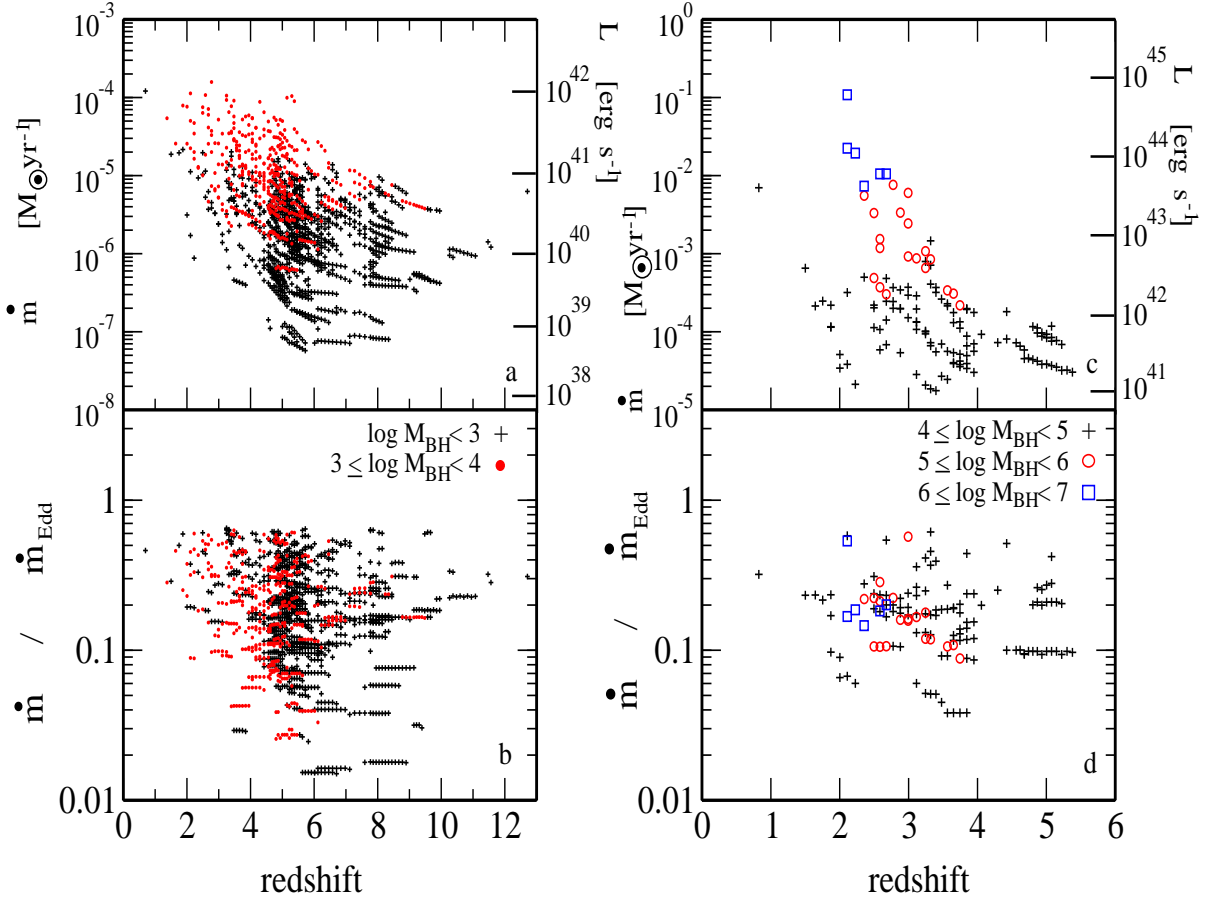


Figure 7. Accretion in the PGA model. Left panels show black holes with mass less than $10^4 M_\odot$, and right panels show more massive black holes. Upper panels: Gas accretion rates and luminosities for all accreting black holes during a random short time interval ($\delta t = t_f - t_i$). Bottom panels: Gas accretion rates at short time intervals as a fraction of the Eddington rate for all accreting black holes. Unlike the FPL model, here most black holes accrete well below the Eddington rate. There are more ($\leq 10^4 M_\odot$) accreting black holes in the PGA model because their growth is not limited by the black hole fundamental plane.

limit specified by the black hole fundamental plane. Instead of invoking AGN feedback in the form of an upper limit on the black hole mass, we incorporate it into the gas accretion efficiency. These feedback mechanisms suppress the accretion efficiency, leading to accretion rates that are 0.01 - 0.8 of Eddington (bottom panel, Fig 7). these lower accretion efficiencies also result in lower luminosities in the PGA model. While for $\sim 10^6 M_\odot$ black holes, the maximum luminosities is $\sim 10^{45} L_\odot$ in the FPL model (upper panel, Fig 6), these black holes have an order of magnitude lower luminosity in the PGA model (upper panel, Fig 7). The maximum accretion rate of the PGA black holes at the redshift of their last accretion is $\sim 0.01 - 0.1 M_\odot/\text{year}$ or $0.8 \dot{m}_{\text{Edd}}$. Thereafter, the gas accretion is extremely damped. Although these SMBHs are far too low a mass to be considered a high luminosity AGNs

analogue, it may be appropriate to link these SMBHs with low luminosity AGNs (Ho 2008). Our approach is in broad agreement with the observations of AGN lifetimes (Hopkins & Hernquist 2009), which show that most local black holes must have gained their mass in no more than a couple of accretion episodes. Again, we point out that Hopkins & Hernquist 2009 discuss their results for more massive black holes ($\geq 10^{7.5} M_\odot$) than those in our study.

3.1.3 Black Hole Growth with Gravitational Wave Recoil

We include gravitational wave recoil from the uniform K1 and lower recoil K2 distributions and reproduce 1,000 merger trees for each kick distribution in

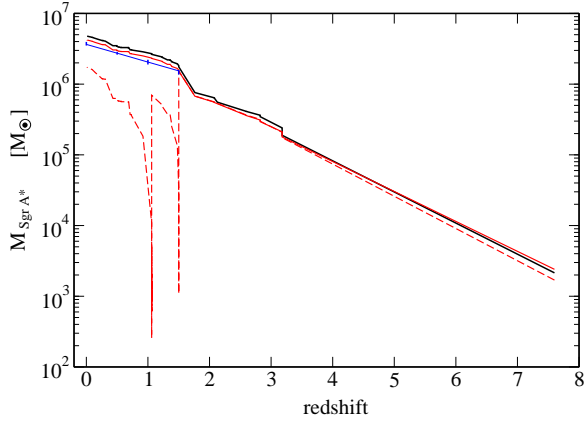


Figure 8. The evolution of Sgr A* in the FPL model for 1000 K1 kick realizations. The black solid line shows the black hole growth when kicks are excluded. Solid and dashed red lines show the black hole growth that produces the largest ($4.3 \times 10^6 M_\odot$) and smallest ($2.0 \times 10^6 M_\odot$) final black hole. The most common black hole mass is $3.9 \times 10^6 M_\odot$ (blue). Also in blue: the $1-\sigma$ spread around the most common value for redshifts $z=1.5$; 1.0 ; 0.5 ; and 0.0 , further showing that the most common mass is near the mass of Sgr A*.

both the FPL and PGA models. This results in 4,000 merger trees presented in figures 8, 9, 10, and 11.

Figure 8 shows results for the K1 distribution in the FPL model. When kicks are excluded, the final black hole mass is $5 \times 10^6 M_\odot$. The largest and smallest black holes at the center of the Milky Way analog are $4.3 \times 10^6 M_\odot$ and $2.0 \times 10^6 M_\odot$, respectively, while the most common black hole mass is $3.9 \times 10^6 M_\odot$. Figure 8 also shows the $1-\sigma$ spread around the most common value for redshifts $z=1.5$; 1.0 ; 0.5 ; and 0.0 , further showing that the typical mass remains near the mass of Sgr A*. In the realization that favors the smallest SMBH mass, the kicks are so large that the black hole is ejected from the center of the Milky Way in two occasions. The reason the FPL model produces a final SMBH mass that so closely matches Sgr A* is quite trivial: it is built into the model that any major merger will grow the SMBH up to the mass dictated by the black hole fundamental plane. Even when the central black hole in the Milky Way analog is only $\sim 100 M_\odot$ at $z=1.1$, there is plenty of time to grow the black hole back to the supermassive range.

This also acts to shift the typical black hole mass toward the merger tree realization with largest final black hole mass. In the case of lower amplitude K2 distribution (with black hole spin axes aligned) this effect is even more pronounced (figure 9). In figure 9, we show the $z \leq 2$ part of the merger tree for the case that excludes kicks, as well as the extrema in final black hole masses, all of which are close to the observed Sgr A* mass.

Gravitational wave recoil matters much more in

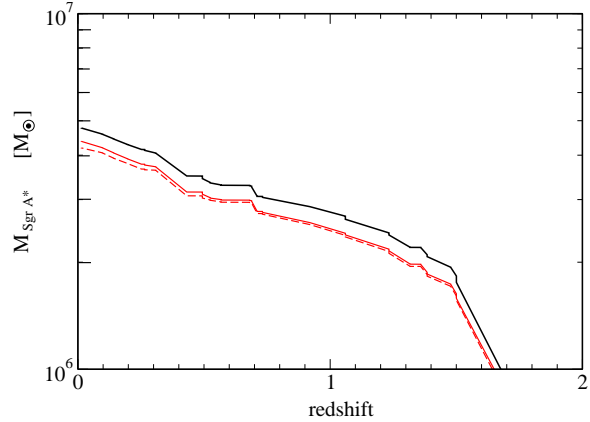


Figure 9. Sgr A* evolution in the FPL model for 1000 K2 kick realizations (lower recoil). Black : the $z \leq 2$ part of the merger tree when kicks are excluded. Solid red: kick realization favoring the largest black hole at the center of Milky Way analog. Dashed red: the kick realization favoring the smallest final black hole. Both the smallest and largest values are close to the observed Sgr A* mass.

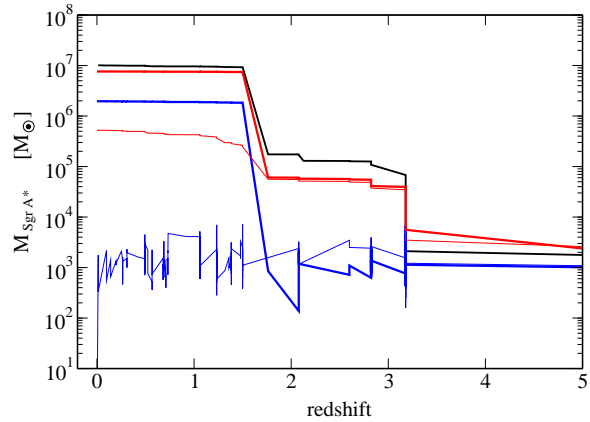


Figure 10. Sgr A* evolution in the PGA model for 1000 K1 and K2 (lower recoil) kick realizations. Black solid line: Sgr A* when kicks are excluded. The red thick and thin lines show the K1 and K2 realizations favoring the largest black holes. The blue thick and thin lines show the K1 and K2 realizations favoring the smallest black holes. Here, the scatter is much larger than in the FPL model, particularly for the higher K1 recoil distribution.

the PGA model, as can be seen in figure 10 which shows the central SMBH mass of the Milky Way analogue as a function of redshift. Although the final black hole mass lies in a much wider range of masses, these outliers in mass are rare. Figure 11 shows the black hole mass with the largest probability at redshifts $z=3.0$ (blue); 1.5 (red); and 0.0 (black) for PGA models. The black line shows that for the lower recoil velocities, K2 case at $z=0$, the typical black hole mass is in the Sgr A* range 90% of the time. Note

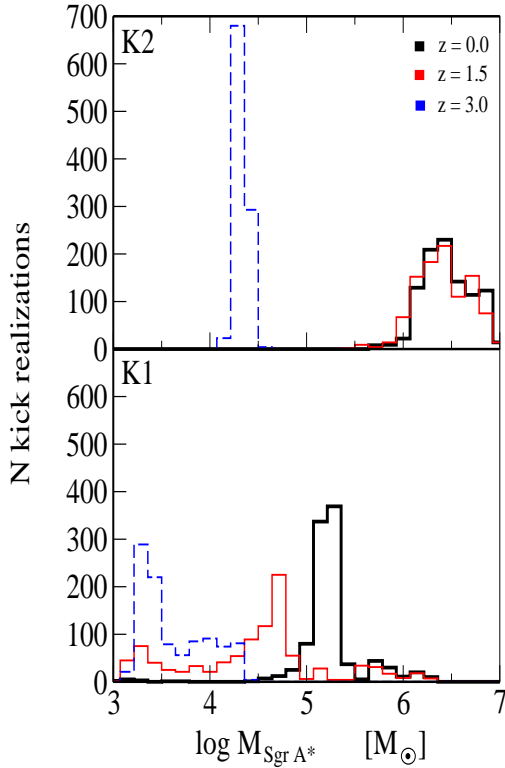


Figure 11. Upper panel: Number of lower recoil K2 realizations in the PGA model where Sgr A* reaches a certain mass at a certain redshift. Bottom panel: Number of K1 realizations in the PGA model where Sgr A* reaches a certain mass at a certain redshift. Histograms are at $z=3.0$ (blue dashed); $z=1.5$ (red thin); and $z=0$ (thick black). In the lower recoil K2 case, Sgr A* reaches the observed value at $z=0$ in more than 90% of kick realizations.

that since it is thought that the black hole spin vectors may align with one another before coalescence (Bogdanovic et al. 2007, Sperhake 2009, Kesden et al. 2010), we consider this our best and most realistic model. If SMBH grows according to the PGA model then kicks must be in the lower range described by K2 distribution. However, this does imply a scatter in the $M-\sigma$ relation at the low mass end.

4 OTHER POPULATIONS OF MASSIVE BLACK HOLES

We distinguish three different massive black hole populations in our merger trees: black holes at the centers of local field dwarf galaxies (other halos in VL-2 outside of the Milky Way halo); rogue black holes scattered through the Milky Way halo (remnants of satellites which merge with Milky Way but do not reach the center in less than Hubble time, Micic et al. 2007, Bellovary et al. 2010); and black holes ejected from their host halos to occupy the intergalactic medium (if

the satellite does reach the center of Milky Way, the following black hole merger might lead to the black hole ejection).

4.1 Massive Black Holes in the Local Dwarfs

For dark matter halo masses above roughly $5 \times 10^{11} M_\odot$, the dark matter halo mass correlates well with the mass of the supermassive black hole (Ferrarese 2002):

$$\frac{M_{\text{BH}}}{10^8 M_\odot} \sim A \left(\frac{M_{\text{DMH}}}{10^{12} M_\odot} \right)^m, \quad (11)$$

where M_{DMH} is the dark matter halo mass, $A=0.1$, and $m=1.65$ defines the slope in the relation. Below this mass, there is tentative evidence that halos are less effective at forming massive black holes, and may even be unable to form them (Ferrarese 2002). To be fair, though, if this relation does hold down to a $10^{11} M_\odot$ halo, the expected $2 \times 10^4 M_\odot$ black hole would be difficult to detect, observationally.

Outside of the Milky Way, there are 35 local field dwarf galaxies in VL-2 identified at $z=0$ in the mass range $10^7 M_\odot - 10^{11} M_\odot$. Figure 12 shows the black hole mass at the centers of these field dwarfs as a function of dark matter halo mass in the FPL (left) and PGA (right) models. Thick black vertical lines represent minimum and maximum values for the black hole mass in 1,000 kick realizations. The Red pluses corresponding to the vertical black lines represent most common mass between minimum and maximum. If a red plus is absent, the most common black hole mass for that halo is zero. Linear fits to the most common masses are presented by red lines. Note that for our linear fits, we exclude those field dwarfs that have ejected their central black holes entirely in more than 50% of kick realizations.

The FPL model predicts an $M_{\text{BH}}-M_{\text{DMH}}$ for field dwarf galaxies in K1 and lower recoil velocities K2 cases as follows.

For FPL K1:

$$\frac{M_{\text{BH}}}{10^8 M_\odot} \sim 0.08 \left(\frac{M_{\text{DMH}}}{10^{12} M_\odot} \right)^{1.14 \pm 0.50}, \quad (12)$$

while FPL lower recoil K2 has a slightly shallower slope:

$$\frac{M_{\text{BH}}}{10^8 M_\odot} \sim 0.05 \left(\frac{M_{\text{DMH}}}{10^{12} M_\odot} \right)^{1.06 \pm 0.41}, \quad (13)$$

The PGA K1 model, on the other hand, predicts:

$$\frac{M_{\text{BH}}}{10^8 M_\odot} \sim 0.002 \left(\frac{M_{\text{DMH}}}{10^{12} M_\odot} \right)^{0.64 \pm 0.36}, \quad (14)$$

and finally, the PGA lower recoil K2 model has the following relation:

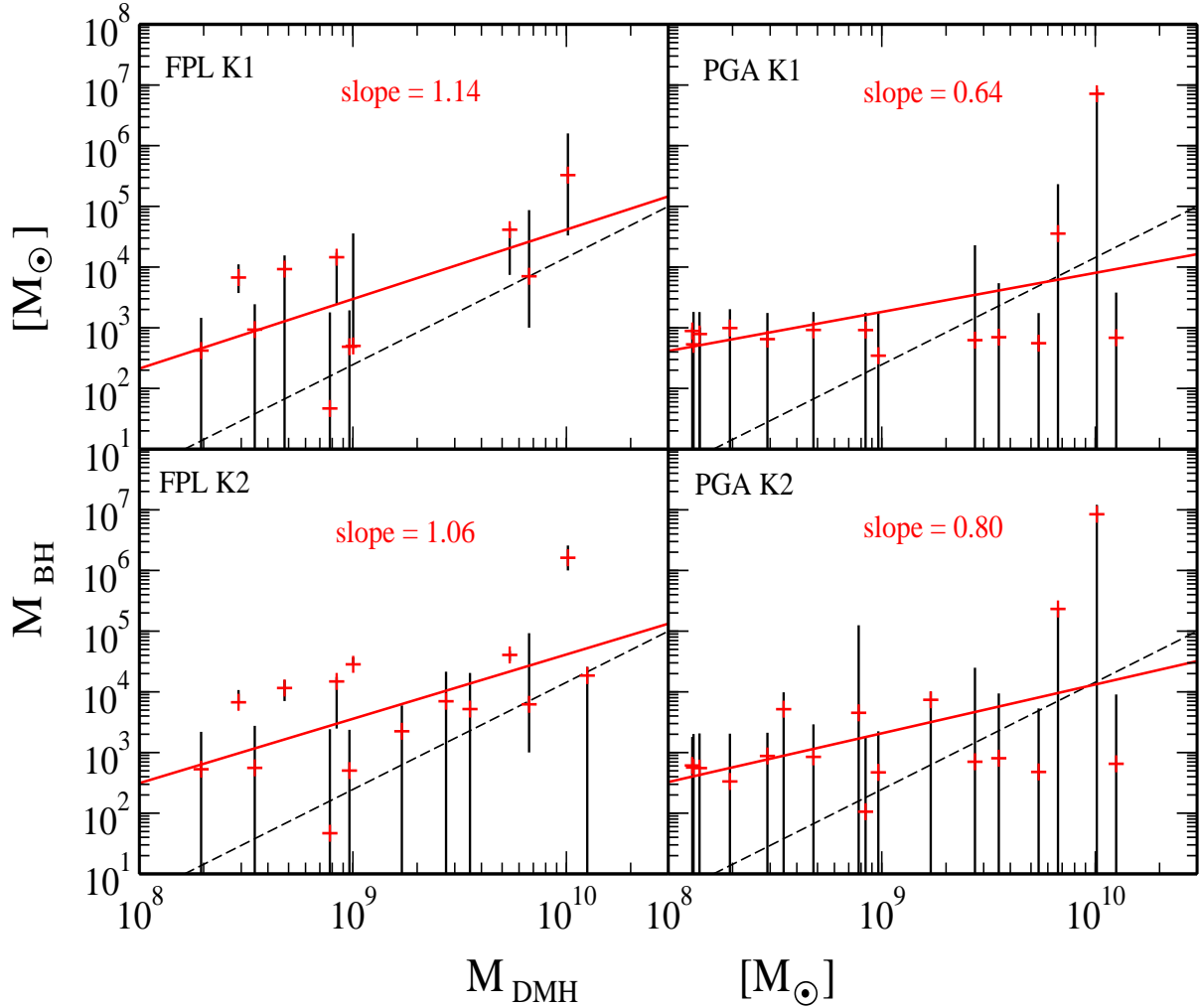


Figure 12. Black hole demography for the FPL K1 model - upper left; FPL lower recoil K2 model - bottom left; PGA K1 - upper right; and PGA lower recoil K2 - bottom right. The dashed line in every panel represents the Ferrarese relation with a slope = 1.65. Red pluses: the most common central black hole mass. For the rest of 35 field dwarf galaxies most common outcome is absence of central massive black hole. Red line: linear fit to the most common black hole masses. Black vertical bars: the scatter in final black hole mass produced by kicks. This would reflect the scatter in relations that connect the central black hole mass with the properties of field dwarf galaxies.

$$\frac{M_{\text{BH}}}{10^8 M_{\odot}} \sim 0.005 \left(\frac{M_{\text{DMH}}}{10^{12} M_{\odot}} \right)^{0.80 \pm 0.36}. \quad (15)$$

A generic prediction of each model is that the slope is shallower than the Ferrarese relation presented by dashed lines in Fig 12. For FPL K1 and lower recoil K2 models, the slope m is 1.14 and 1.06, close to $M_{\text{DMH}} / M_{\text{BH}} = 10^5$. PGA models predict an even shallower slope of 0.64 in K1 and 0.80 in the case of lower recoil velocities K2. This tests the PGA model by predicting a substantially flatter mass function for lower mass SMBH. We do point that these differences

between FPL and PGA models might be insignificant, considering that scatter around the linear fits is substantial.

4.2 Rogue Massive Black Holes in the Milky Way

Rogue black holes are carried into the Milky Way halo by their host satellites, but have halo merger time scales longer than a Hubble time. Over the span of the simulation, the Milky Way accretes 669 satellite halos which host a black hole, and 249 have orbital

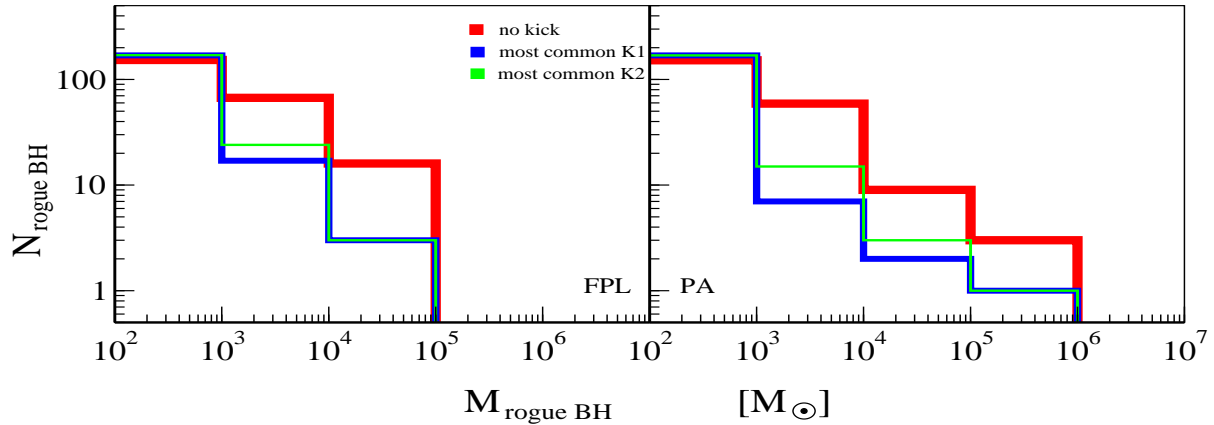


Figure 13. Number of rogue black holes spread through the Milky Way halo as a function of mass, for the FPL (left panel) and PGA (right panel) models. Red histograms – the merger tree that excludes black hole kicks. Blue histogram – the most common merger tree in the K1 kick distribution. Green histogram – the most common merger tree for the lower recoil K2 case. These black holes originate from the centers of satellites that merged with the Milky Way analogue but had merger timescales larger than a Hubble time. As the black holes fail to reach the Milky Way center, they orbit in the Milky Way halo. These models predict hundreds of rogue black holes with masses reaching up to $\sim 200,000 M_{\odot}$.

decay times that are longer than a Hubble time (see figure 1 and figure 4 for the merger time scale, merger rate and mass ratios of these halos). By redshift zero, then, these halos are still orbiting at significant distances from the center of Milky Way – and although the halos themselves have been stripped by the primary potential, they still host massive black holes. Figure 13 shows the number of rogue black holes as a function of mass for the FPL (left) and PGA (right) models. As before, the upper limit for black hole mass excludes kicks and is presented in red in both panels. For each kick model, we also present the number of rogue black holes with the typical mass over the realizations. The PGA model predicts that there should be at least one massive rogue black hole in the Milky way halo with mass in range $10^5 M_{\odot}$ – $10^6 M_{\odot}$.

The distance from the Milky Way center in all models is correlated with the redshift at which galaxies merge (figure 14). If the merger occurred early at high redshift, the black hole had more time to sink to the center, and for mergers close to $z=0$, the black hole has just entered Milky Way halo. The redshift at which the halo merges with the Milky Way also marks the end of the rogue black hole growth. Hence, rogue black holes that enter the Milky Way at later times have had more time to grow, and will be more massive than those accreted through early mergers. Figures 15 and 16 show how rogue black hole mass, satellite merger redshift, and distance from the Milky Way are correlated. Figure 15 represents the FPL model and figure 16 represents the PGA model. K1 realizations are shown in the left panels, and lower recoil K2 realizations in the right.

Unfortunately, both figures clearly show that the most massive rogue black holes are furthest away and

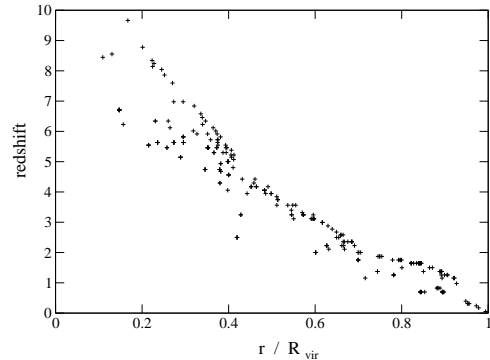


Figure 14. Redshift of satellite mergers with the Milky Way analogue as a function of the current position in the Milky Way halo. Those satellites that merged with the Milky Way at high redshift have sunk closer to the Galactic center. In later mergers, the satellites have just entered the Milky Way and are closer to the virial radius. Since each satellite potentially carries a black hole, this figure shows the distance of rogue black holes from the center of the Milky Way.

may be very difficult to observe. We estimate the Bondi accretion onto these black holes to determine how observable they may be and we describe the process below.

There is sufficient evidence that the halos of galaxies, from massive ellipticals to isolated spirals, can host diffuse hot halo gas (Matthews & Brighenti 2003, O’Sullivan et al. 2001, Pedersen et al. 2006). As these black holes orbit within the primary halo, they can accrete from this ambient hot halo gas via

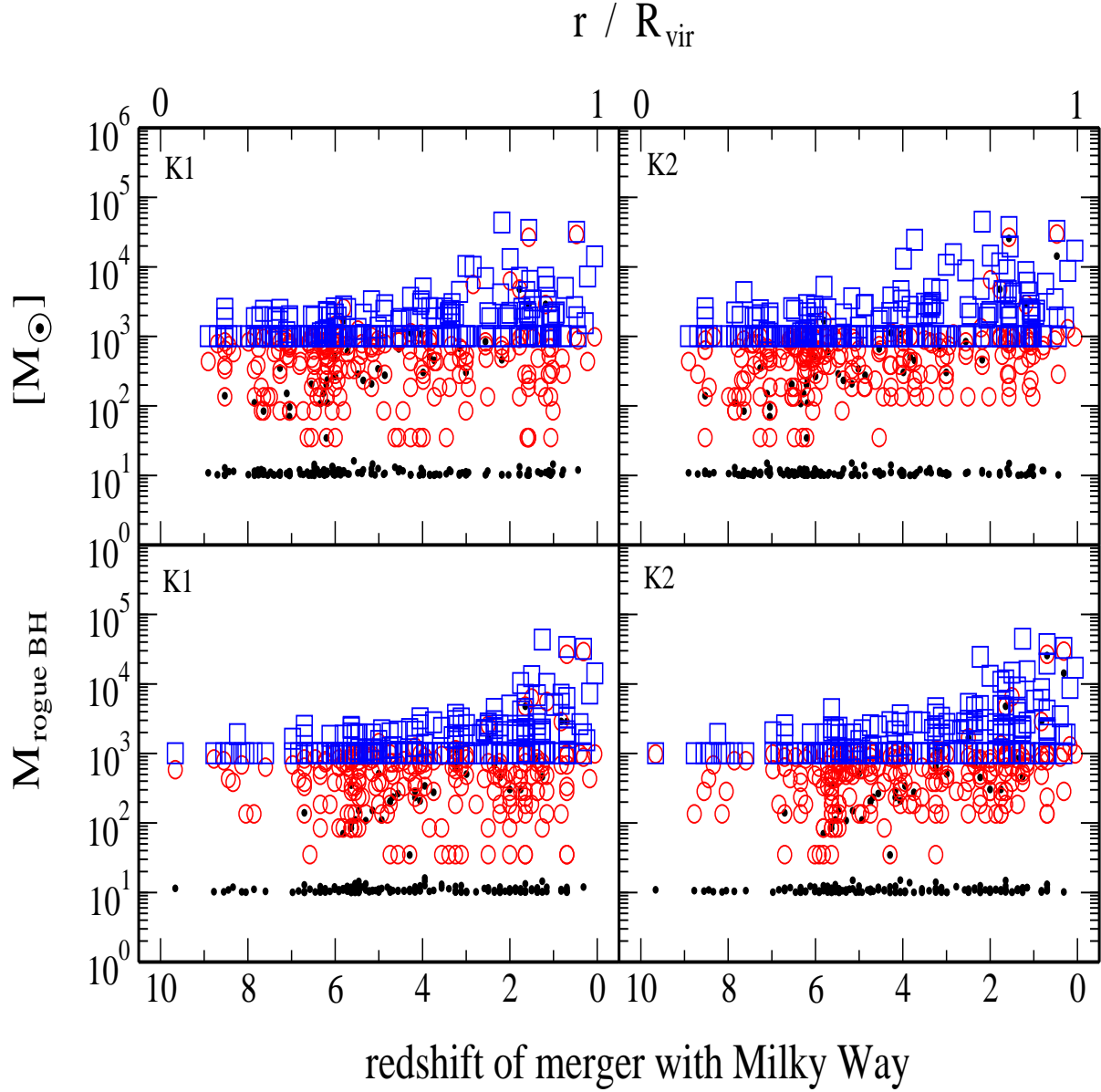


Figure 15. Rogue black hole mass as a function of Galactic distance and progenitor halo redshift for the FPL model. Left panels: the K1 distribution. Right panels: the lower recoil K2 case. The blue squares represent the most massive rogue black holes; red circles represent the typical black hole mass, and black dots represent the lightest. Those black holes carried by satellites that merge later have had more time to grow, so the rogue black hole mass correlates with both distance from the center and merger redshift. The most massive rogues reach $\sim 30,000 M_{\odot}$ at $0.8 - 1.0$ of virial radius.

Bondi-Hoyle accretion. Here, the mass accretion rate can then be described by:

$$\dot{M}_{\text{BH}} = \frac{4\pi G^2 M_{\text{BH}}^2 \rho_{\text{ISM}}}{(c_s^2 + v^2)^{3/2}}, \quad (16)$$

where ρ_{ISM} is the density of the halo gas, c_s is the gas sound speed, and v is the velocity of the black

hole. For these rogue black holes, we add this more quiescent form of accretion from the time the black hole has entered the virial radius of the halo in order to determine whether any may be visible today. To model the hot halo gas, we use a technique outlined in Sinha & Holley-Bockelmann (2009). In short, we assume it has an isothermal density profile consis-

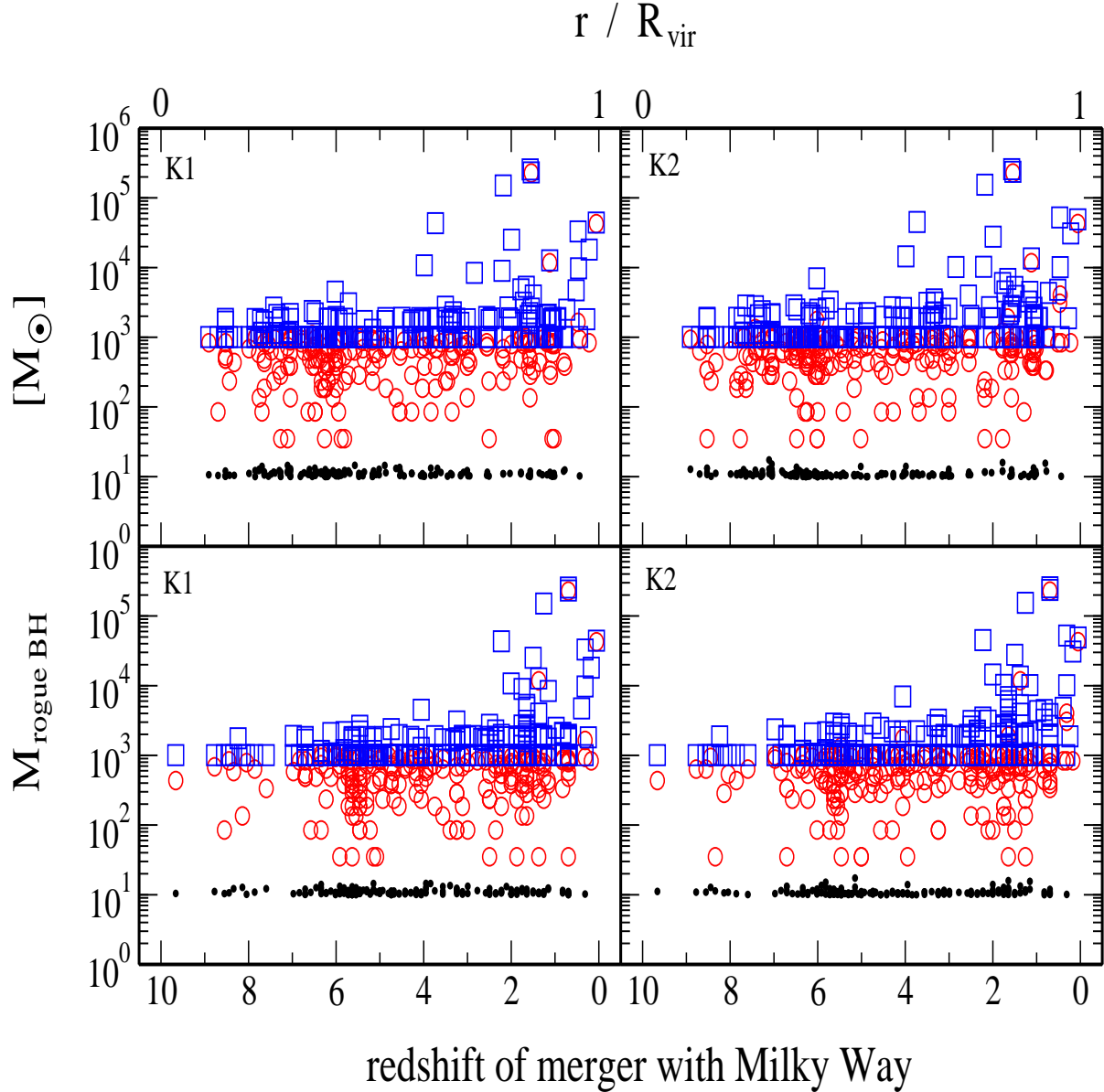


Figure 16. Rogue black hole mass as a function of Galactic distance and progenitor halo redshift for the PGA model. Left panels: the K1 distribution. Right panels: the lower recoil K2 case. The blue squares represent the most massive rogue black holes; red circles represent the typical black hole mass, and black dots represent the lightest. The most common rogue black hole mass remains at the initial black hole seed mass, but a number of massive rogue black holes are greater than $10,000 M_{\odot}$. The most massive is $M_{\text{rogue}} \sim 230,000 M_{\odot}$ at 225 kpc from the Galactic Center (0.8 – 0.9 of virial radius).

tent with X-ray observations of halo gas in ellipticals (Matthews & Brighenti 2003), and that the ideal gas is in hydrostatic equilibrium with the gravitational potential of the halo. We assume a gas core radius of $0.3R_s$, where R_s is the scale radius of the NFW halo, and that the gas temperature is the virial temperature at the virial radius. This yields a central gas temper-

ature of $\sim 2 \times 10^6 K$ for a dark matter halo of mass $2 \times 10^{12} M_{\odot}$, which is also consistent with observations (Pedersen et al. 2006). At redshift zero, we assume the black holes are on bound elliptical orbits of eccentricity 0.8 to match simulation predictions for satellite mergers (e.g. Ghigna et al. 1998, Sales et al. 2007).

By redshift zero, these black holes will have grown

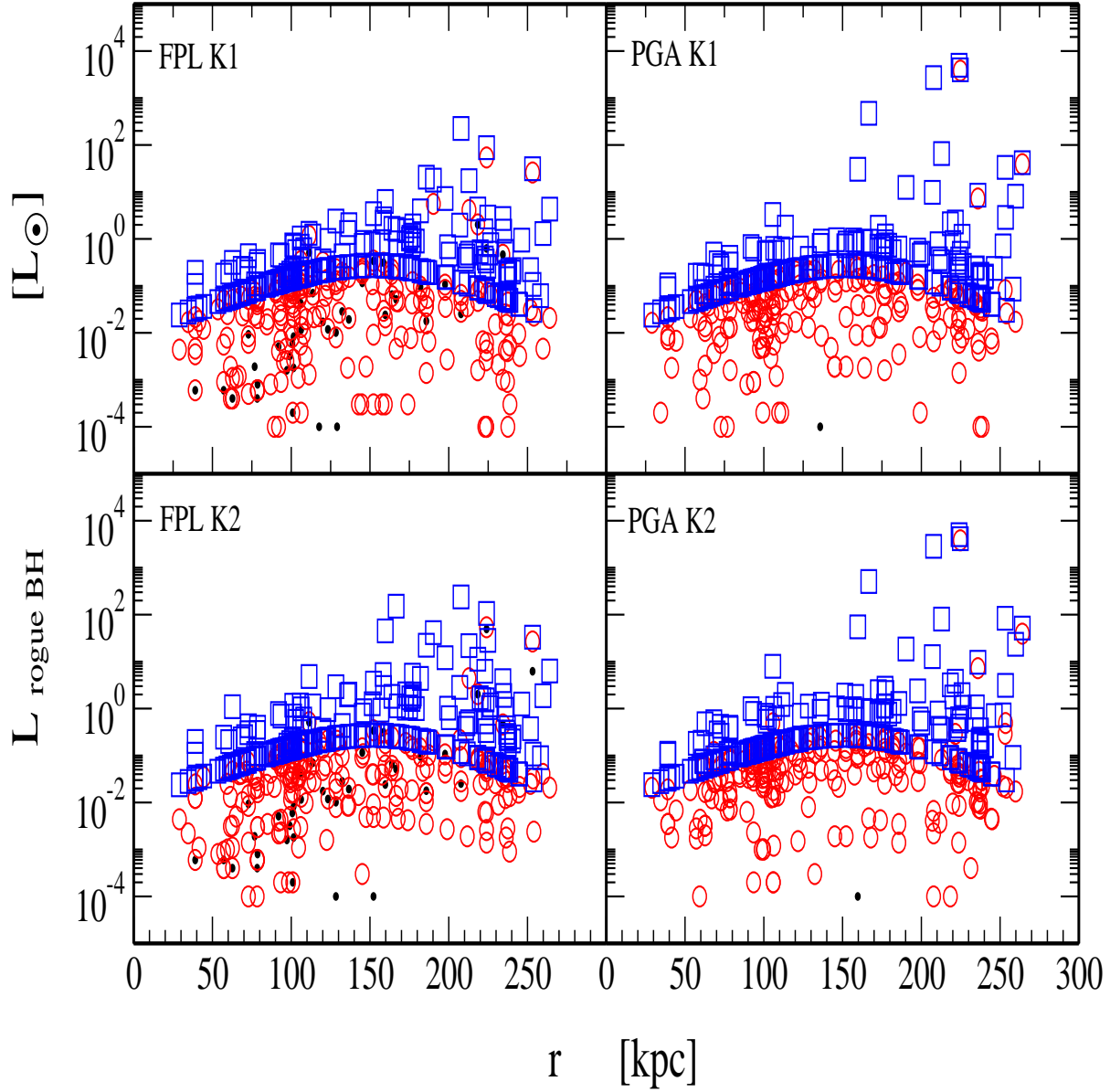


Figure 17. Bolometric luminosity of rogue black holes as a function of distance from the primary halo center for the FPL (left) and PGA (right) models. The K1 case is on the upper panels and the lower recoil K2 case on the bottom. Blue squares represent the most massive rogue black holes; red circles represent the typical black hole mass, and black dots represent the smallest. Black holes are assumed to accrete via a Bondi-Hoyle mechanism from the ambient gas in the Milky Way. Most rogue black holes are well below solar luminosity, but a few are expected to be luminous X-ray sources (just under the ULX cut-off) that reside in the outskirts of the Milky Way halo. The most massive of them is in PGA model and has a luminosity of $4000 L_{\odot}$.

to a new mass, M_{rogue} , and will have a new accretion rate from equation 16. The radiated luminosity from this process can be determined from $L_{\text{rogue}} = \eta \dot{M}_{\text{BH}} c^2$, where η describes how efficiently mass is converted to energy; the standard assumption for an accretion disk

around a spinning black hole sets $\eta \sim 0.1$ (Shakura & Syunyaev 1973). We find that our most massive rogue black hole $M_{\text{rogue}} = 227,643 M_{\odot}$, residing at 225 kpc from the Galactic center, can radiate at $3,834 L_{\odot}$ (figure 17, PGA panels on the right), making it

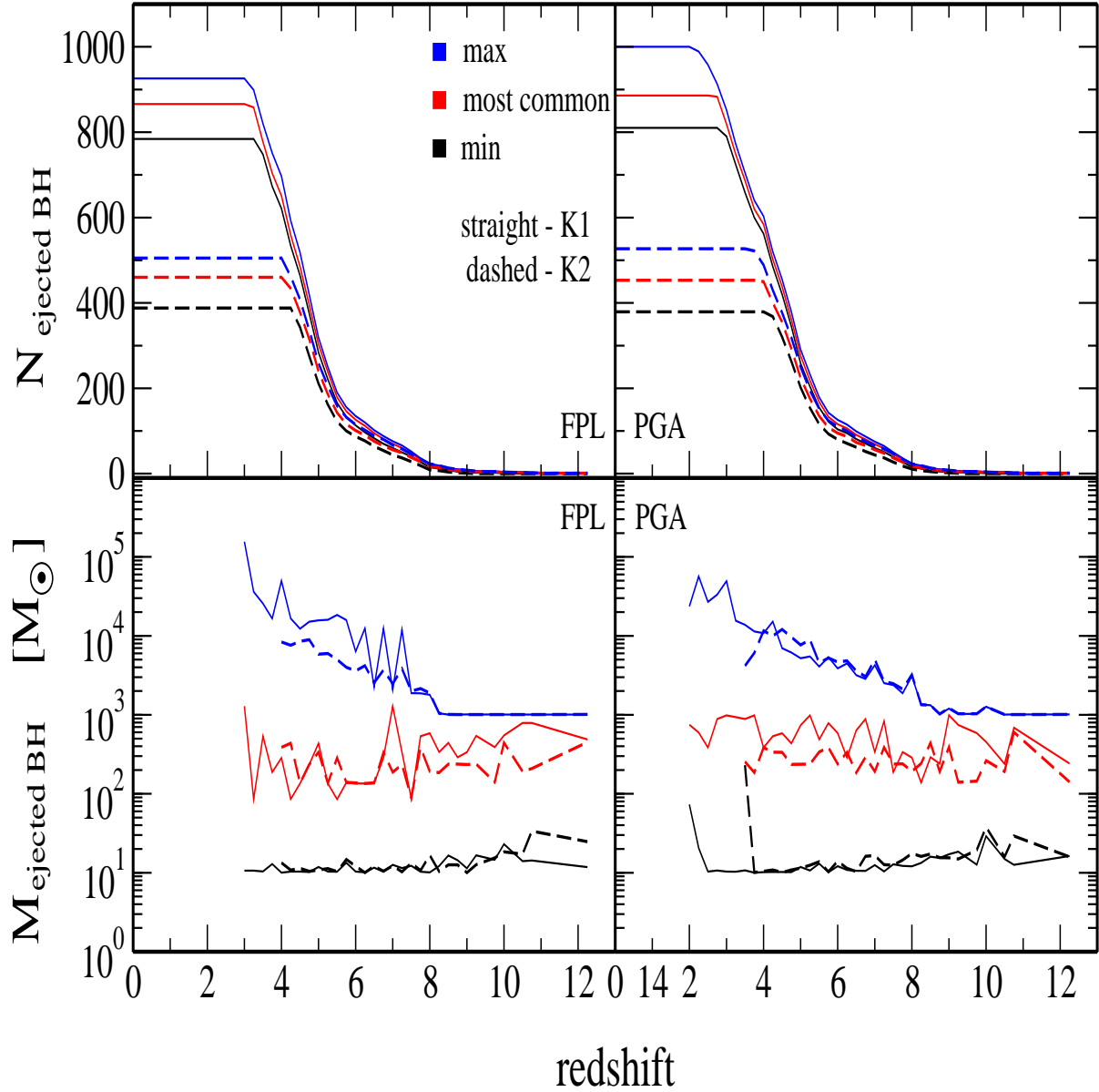


Figure 18. Upper panels: The cumulative number of ejected black holes as a function of redshift for all halos in VL-2 for the FPL (left) and PGA (right) models. The K1 (solid line) and lower recoil K2 (dashed line) kick distributions are shown. In blue is the maximum cumulative number of ejected black holes; in red is the typical number; in black – the minimum. Lower panels: The black hole mass of the ejected population. The colors are the same as in the top panels.

somewhat fainter than the brightest ULXs; the fact that the hot halo gas is so tenuous at these radii is what accounts for the relatively low luminosity.

However, if these rogue black holes are common, they will be observable in the outskirts of the Milky Way halo with Chandra, and the most luminous can have sufficient signal-to-noise for spectral characterization. Note, though, that a significant fraction of these

may have advection-dominated accretion flows, rather than thin accretion disks, and hence η may be much less than 0.1; this would naturally make the black hole less luminous, but with a harder spectral signature. It has also been suggested that rogue black holes in the molecular or cold neutral part of the ISM should be more easily detected in the radio than in X-rays (Maccarone 2004, Maccarone et al. 2005). Maccarone 2005,

for example, calculates that a $2,600 M_{\odot}$ black hole should be observable with LOFAR (above $30\mu\text{Jy}$) in the radio out to about 15 kpc – much closer than the most massive rogue black hole in our model. Assuming larger black hole velocities and a more efficient Bondi accretion rate, rogue black holes may be observed at even larger distances. Even if they are not observable electromagnetically, they may be detected by mesolensing (di Stefano 2007).

4.3 Ejected Massive Black Holes

As the SMBH grows, incoming black holes are kicked from the center of the host halo, forming a population of “ejected” black holes. Figure 18 shows the cumulative number of black holes lost from the merger tree due to kicks larger than the escape velocity in the top panels, and the ejected black hole mass as a function of redshift on the bottom panels. Again, we show the FPL model on the left and our PGA model on the right. The redshift of the last SMBH ejection is between $z=2-3$ for the PGA model, and between $z=3-4$ for the FPL model. When we compare the difference in total numbers of ejected BHs between K1 and lower recoil K2 realizations (upper panels in figure 18), both the FPL and PGA model predict the the K1 case ejects up to 50% more black holes. The average masses of ejected black holes are similar in the FPL and PGA models (bottom panels in figure 18) with the most common ejected black hole of $100 - 1,000 M_{\odot}$.

The mass ratio of merging black holes sets the kick amplitude, with large differences between the incoming black hole mass creating a small kick. The typical number of ejected black holes per realization as a function of mass ratio is presented in figure 19. The FPL and PGA distributions are again very similar regardless of the kick distribution. The main difference is that higher mass ratio encounters are more common in the PGA K1 model. Since the growth of black holes in the FPL model is very efficient – at Eddington rate – the incoming black holes grow faster and this decreases the mass ratio when the merger occurs. Hence, there are more mergers at $q \leq 0.3$ in FPL K1 and more mergers at $q \geq 0.3$ in PGA K1.

Some of the ejected massive black holes might contribute to the rogue black hole population. Micic et al. 2006 has shown that high redshift ejections of black holes from their host halos in the Local Group type environment could lead to their capture by Milky Way potential. Tracking these black holes are beyond the scope of this paper and will be addressed in future work.

5 DISCUSSION AND CONCLUSIONS

Using a very high resolution small volume cosmological N-body simulation (Via Lactea II), we construct

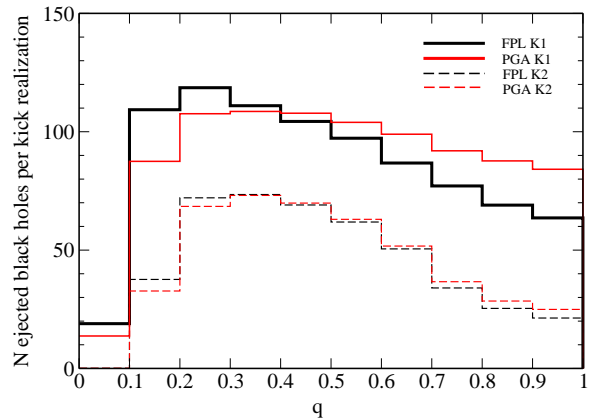


Figure 19. Number of ejected black holes per realization as a function of the mass ratio of the merging black holes. Black lines represent the FPL model, and red lines represent the PGA model. Thick lines show the K1 distribution, while thin dashed lines present the lower recoil K2. Since the K1 model yields on average an order of magnitude larger kick velocities than K2 lower recoil model, the number of ejected black holes is larger for K1.

the merger history of black holes in low mass dark matter halos in a Local Group analog. We found that the method used to estimate the dynamical friction timescale makes a large difference in the total rate and redshift distribution of black hole mergers (see also Holley-Bockelmann et al. 2010). In particular, for example, an N-body based dynamical friction estimate (Boylan-Kolchin 2008) yields longer merger timescales than does Chandrasekhar dynamical friction. These larger, more realistic merger timescales will postpone black hole mergers to lower redshifts. Moreover, if most of the black hole growth is tied to gas accretion that is activated by major mergers, then using Chandrasekhar dynamical friction will overestimate the black hole mass.

We studied the growth and merger rate of black holes from seeds at redshift ~ 20 to low mass SMBHs at redshift zero, analytically incorporating the important sub-resolution physics to model the black hole dynamics and gas accretion. We find that having a constant mass black hole seeds, or a narrow BHMF leads to nearly equal mass ratio black hole mergers. These mergers have largest gravitational wave recoil velocities, which eject the black holes from their host galaxies and suppresses SMBH growth. A wider range BHMF presents far fewer problems in growing SMBHs, even when the black holes spins are large.

Many groups are beginning to explore the formation and evolution of massive supermassive black holes in large volume cosmological volumes, with a sophisticated and self-consistent treatment of the sub-grid physics (e.g. Croton et al. 2006, Sijacki et al. 2007, di Matteo et al. 2008, Sijacki et al. 2009). With larger simulation volumes, these simulations are capable of

forming hundreds of massive SMBHs at the centers of massive elliptical galaxies and clusters of galaxies. In fact, the FPL model we adopt is a semi-analytic model (Somerville et al. 2008) resulting from these techniques. Due to high computational cost, however, the same numerical approach has not been applied in smaller cosmological volumes where the bulk of the halo evolution is non-linear. Here, high redshift dwarf galaxies merge to form the Local Group galaxies, and massive black holes have masses well below $10^7 M_\odot$.

We use small volume nbody simulations and apply two semi-analytic recipes for SMBH growth. One class of models is always limited by the black hole fundamental plane (FPL). Here, the growing black hole mass is a function of the total stellar mass in the galaxy bulge. This approach has successfully produced SMBHs in massive galaxies. We show that the FPL model can also be used for black hole growth in small volumes. In particular, black hole mergers combined with a) gas accretion in a quasar mode and b) a time averaged Bondi-Hoyle accretion rate of $7 \times 10^{-4} M_\odot \text{yr}^{-1}$ in a radio mode, can produce the observed mass of the Sgr A* SMBH. Today, the observed Sgr A* accretion rate is an order of magnitude less efficient than this radio mode accretion rate, but this may not be unreasonable, since the Milky Way is not considered an AGN anymore. Other low mass AGNs in the local Universe are observed to have 10 - 100 times more efficient gas accretion. The FPL model, by design, guarantees the formation of a fundamental plane black hole. However, in reality, not every galaxy has such a system, due to the competition between black hole growth and nuclear star cluster formation in low mass spheroids.

We have proposed an alternative method which could provide deeper insight into the formation of the lightest supermassive black holes ($\leq 10^7 M_\odot$) by incorporating growth prescriptions calculated in small scale merger simulations. Gas accretion onto the black hole is always suppressed by stellar or AGN feedback, and depends on the structure of the gas, as well as the microphysics (such as turbulence, fully relativistic magnetohydrodynamics, etc) that is currently physically beyond modeling. Our model provides a framework into which the microphysics can easily be incorporated once simulations and observations reveal the nature of these processes. In contrast, in the FPL model, these effects are irrelevant, since gas accretion occurs in the same manner in all $\leq 10:1$ galaxy mergers. The final outcome is always a fundamental plane black hole since feedback rapidly drives the evolution of fundamental plane rather than the growth of black holes. In the PGA model, we can incorporate an accretion efficiency parameter into the gas accretion prescription to make black hole growth less efficient for stronger feedback and vice versa. We use a formalism that relates the gas accretion efficiency to galaxy merger ratios; gas accretion is most efficient for major mergers and negligible for minor mergers (Cox et al. 2008).

In addition, minor mergers will last much longer than equal mass mergers. When these two effects combine, the PGA model produces short bursts of high rate gas accretion for equal mass mergers, and long, slow gas accretion for 10:1 mass ratio mergers. As a result, most black holes in the PGA model never reach the Eddington rate.

We also modeled the effect of gravitational wave recoil on assembling the lightest SMBHs. One way to mitigate gravitational wave recoil is to increase the black hole merger symmetry; smooth dense gas, for example, may quickly align the spin vectors of each SMBH before coalescence (Bogdanovic et al. 2007, Dotti et al. 2010). In order to understand how damaging gravitational wave recoil can be, and to pin down the epoch that a growing black hole is most vulnerable to recoil, we do not pre-select the merger configurations with the lowest recoils in K1 and select spins aligned to the orbital angular momentum in lower recoil model K2. In previous work, when black holes are merging in massive stellar systems, the large gravitational potential creates large escape velocities. Hence, a K2 kick distribution with much lower recoil velocities helps retain the central black holes (Volonteri et al. 2010). In our merger tree, most of the dark matter halos have masses below $10^{10} M_\odot$, and the typical halo mass is $10^7 M_\odot - 10^9 M_\odot$. Since the escape velocities in these systems are below 100 km s^{-1} , even the moderate kicks will eject the SMBH. When gravitational recoil is included in the FPL model, the final black hole mass is unaffected in most cases. This is the consequence of the FPL requirement of a very high gas accretion efficiency. Even in the most damaging K1 realization where the black hole is ejected twice from the merger tree, the accretion of gas is so efficient that a $\sim 100 M_\odot$ black hole that is ushered to the center has time to grow to $2 \times 10^6 M_\odot$. When gravitational recoil is included in the PGA model, the final mass of the central black hole in the K1 realizations is lower by roughly an order of magnitude than in K2 (lower recoil model). 90 % of the K2 realizations are in the Sgr A* mass range. PGA model predicts that kicks have to follow lower distribution of gravitational recoil velocities, K2.

When we look at the mass of the black holes at the centers of local field dwarf galaxies, none of the models, FPL or PGA, matches the extrapolation of the Ferrarese (2002), relation which relates black hole masses to the masses of host dark matter halos. Even when we remove gas accretion as a mechanism for black hole growth, their masses will be larger than predicted by Ferrarese relation as the result of seed black hole mergers, despite the fact that the initial black hole seeds were Pop III remnants and therefore considered light seeds. It is possible that the black hole fundamental plane exists for low mass SMBHs in field dwarf galaxies, but it may simply have a different slope than for high mass SMBHs; indeed this was alluded to in the original Ferrarese work. We do find a shallower

slope in all models. In FPL, the slope is close linear and tracks the following proportion: $M_{\text{DMH}} / M_{\text{BH}} = 10^5$. The PGA model predicts an even shallower slope $-0.64 - 0.80$ – although the scatter caused by gravitational wave recoil makes it hard to distinguish between FPL and PA. Note that gas consumption in field dwarf galaxies may favor nuclear star cluster formation rather than a massive black hole. Both FPL and PGA models are consistent with this picture since roughly half the dwarfs contain no central black hole, though the PGA models predict more empty halos on average than FPL. It is important to note that the black hole demographics in the dwarf galaxy regime is critical to distinguish between the FPL and PGA models.

We also identified two massive rogue black hole populations. First, we find ejected black holes, or black holes with kick velocities larger than the host halo escape velocity. We will address the properties of this population with a detailed treatment of their dynamics in the future. The second are rogue black holes from the remnants of satellites that had merger timescales longer than a Hubble time. We find hundreds of these rogue black holes at distances of ~ 200 kpc from the galactic center and with masses from $10 - 10^5 M_{\odot}$ (depending on the model). The most massive of these may be detected in X-ray and are possible mesolensing candidates. These two populations of black holes, which have quite different formation mechanisms, might not be easily disentangled. It is possible that a growing primary halo may recapture black hole ejected by recoil, in which case both populations occupy a similar parameter space (Micic et al. 2006).

In conclusion, our model successfully reproduces Sgr A* without limiting the black hole growth to the black hole fundamental plane. It predicts that kicks have to follow lower recoil velocity distribution (K2). It also predicts a substantially flatter mass function (slope = $0.64 - 0.8$) for lower mass SMBH in local field dwarfs. It predicts Milky Way rogue black holes, and a population of ejected black holes. This model provides cosmological framework into which the results of small scale simulations can easily be incorporated in the future. At this point, the model is limited only by the lack of understanding of how various feedback mechanisms couple with each other and with the gas accretion onto the black hole. There is ample ground to cover in this respect. As one example, Ostriker et al. (2010) claim that all previous studies of SMBH growth may overestimate the final black hole mass by \sim two orders of magnitude by treating only the energy part of AGN feedback, neglecting the importance of momentum and mechanical feedback. Hopefully, this will be resolved in the future.

One issue is how well the VL-2 simulation represents the Milky Way merger history. The reality is that VL-2 represents one out many possible evolutionary histories of the Local Group, and not necessarily the correct one. The fact that only major mergers acti-

vate the quasar mode means that the number of major mergers each galaxy goes through has a huge impact on the black hole accretion history. This underlines the importance of approaching the problem of Sgr A* growth statistically by simulating hundreds of highly resolved small simulation volumes. To resolve thousands of Milky Way mass halos with VL-2 resolution, gas physics, and black hole dynamics implemented on the fly will be computationally too expensive in the near future.

ACKNOWLEDGMENTS

MM acknowledges support from ARC DP DP0665574. KHB acknowledges the support of NSF Career Grant AST-0847696, as well as the supercomputing support of Vanderbilt's Advanced Center for Computation Research and Education, and NASA's Pleiades and Columbia clusters. This project benefited from interactions during the Aspen Center for Physics Summer Program.

REFERENCES

- Aguilar, L.A., White, S.D.M., 1986, *ApJ*, 307, 97
- Alexander, D.M., Smail, I., Bauer, F.E., Chapman, S.C., Blain, A.W., Brandt, W.N., Ivison, R.J., 2005, *Natur*, 434, 738A
- Abel, T., Bryan, G., Norman, M., 2000, *ApJ*, 540, 39
- Abel, T., Bryan, G., Norman, M., 2002, *Sci*, 295, 93A
- Adams, F.C., Graff, D.S., Richstone, D.O., 2001, *ApJ*, 551L, 31A
- Baes, M., Buyle, P., Hau, G.K.T., Dejonghe, H., 2003, *MNRAS*, 341L, 44B
- Baker, J. G., et al. 2007, *ApJ*, 668, 1140B
- Begelman, M.C., Blandford, R.D., Rees, M.J., 1980, *Natur*, 287, 307
- Begelman, M.C., Rees, M.J., 1978, *MNRAS*, 185, 847B
- Bellovary, J. M., Governato, F., Quinn, T.R., Wadsley, J., Shen, S., Volonteri, M., 2010, *MNRAS*, 721L, 148B
- Bender, R., Kormendy, J., Bower, G., 2005, *ApJ*, 631, 280
- Berczik, P., Merritt, D., Spurzem, R., Bischof, H.P., 2006, *ApJ*, 642L, 21B
- Binney, J., Tremaine, S., 1987, *Galactic Dynamics* (Princeton: Princeton Univ. Press)
- Bogdanovic, T., Reynolds, C.S., Miller, M.C., 2007, *ApJ*, 661L, 147B
- Boker, T., Laine, S., van der Marel R.P., Sarzi, M., Rix, H.-W., & Ho, L.C., Shields, J.C., et al., 2002, *AJ*, 123, 1389
- Booth, C. M., Schaye, J., 2009, *MNRAS*, 398, 53B
- Boylan-Kolchin, M., Ma, C.P., Quataert, E., 2008, *MNRAS*, 383, 93B
- Bromm, V., Coppi, P.S., Larson, R.B., 1999, *ApJ*, 527, L5
- Bromm, V., Loeb, A., 2003, *ApJ*, 596, 34B
- Bromm, V., Loeb, A., 2004, *NewA*, 9, 353B
- Bullock, J.S., Kollat, T.S., Sigad, Y., Somerville, R.S., Kravtsov, A.V., Klypin, A.A., Primack, J.R., Dekel, A., 2001, *MNRAS*, 321, 559B
- Burkert, A., Silk, J., 2001, *ApJ*, 554L, 151B

- Campanelli, M., Lousto, C.O., Zlochower, Y., Merritt, D., 2007, *gr.qc*, 2133C
- Cattaneo, A., Haehnelt, M.G., Rees, M.J., 1999, *MNRAS*, 308, 77C
- Colpi, M., Mayer, L., Governato, F., 1999, *ApJ*, 525, 720C
- Colpi, M., Dotti, M., Mayer, L., & Kazantzidis, S. 2007, *ArXiv e-prints*, 710, *arXiv:0710.5207*
- Cote, P., et al., 2006, *ApJS*, 165, 57
- Cox, T. J., Jonsson, P., Somerville, R. S., Primack, J. R., Dekel, A., 2008, *MNRAS*, 384, 386
- Croton, D.J., Springel, V., White, S.D.M., De Lucia, G., Frenk, C.S., Gao, L., Jenkins, A., Kauffmann, G., Navarro, J.F., Yoshida, N., 2006, *MNRAS*, 365, 11C
- David, L.P., Durisen, R.H., Cohn, H.N., 1987, *ApJ*, 313, 556D
- Dekel, A., et al. 2009, *Natur*, 457, 451D
- Diemand, J., Kuhlen, M., Madau, P., 2007, *ApJ*, 667, 859D
- Diemand, J., Kuhlen, M., Madau, P., Zemp, M., Moore, B., Potter, D., Stadel, J., 2008, *Natur*, 454, 735D
- Di Matteo, T., Croft, R.A.C., Springel, V., Hernquist, L., 2003, *ApJ*, 593, 56D
- Di Matteo, T., Springel, V., Hernquist, L., 2005, *Natur*, 433, 604D
- Di Matteo, T., Colberg, J., Springel, V., Hernquist, L., Sijacki, D., 2008, *ApJ*, 676, 33D
- Di Steffano, R., 2007, *astro-ph/0712.3558*
- Dotti, M., Colpi, M., Haardt, F., Lucio, M., 2007, *MNRAS*, 379, 956D
- Dotti, M., Volonteri, M., Perego, A., Colpi, M., Ruskowski, M., Haardt, F., 2010, *MNRAS*, 402, 682D
- Ebisuzaki, T., Makino, J., Okumura, S.K., 1991, *Natur*, 354, 212E
- Escala, A., Larson, R.B., Coppi, P.S., Mardones, D., 2005, *ApJ*, 630, 152
- Fan, X., 2005, *gbha.conf*, 75F
- Fender, R.P., Belloni, T.M., Gallo, E., 2004, *MNRAS*, 355, 1105
- Ferrarese, L., Merritt, D., 2000, *ApJ*, 539L, 9F
- Ferrarese, L., 2002, *ApJ*, 578, 90F
- Ferrarese, L., et al. 2006, *ApJ*, 644L, 21F
- Gebhardt, K., et al. 2000, *ApJ*, 539L, 13G
- Gebhardt, K., et al. 2001, *AJ*, 122, 2469
- Ghez, A.M., et al., 2008, *ApJ*, 689, 1044G
- Ghigna, S., Moore, B., Governato, F., Lake, G., Quinn, T., Stadel, J., 1998, *MNRAS*, 300, 146
- Glover, S.C.O., 2010, *astro-ph/1007.2763*
- Gnedin, N. Y., 2000, *ApJ*, 542, 535G
- Gonzalez, J.A., Hannam, M., Sperhake, U., Bruggmann, B., Husa, S., 2007, *PhRvL*, 98w1101G
- Gonzalez, J.A., Sperhake, U., Bruggmann, B., Hannam, M., Husa, S., 2007, *PhRvL*, 98l1101G
- Granato, G.L., Silva, L., Monaco, P., Panuzzo, P., Salucci, P., De Zotti, G., Danese, L., 2001, *MNRAS*, 324, 757G
- Greenstein, J.L., Matthews, T.A., 1963, *AJ*, 68S, 279G
- Haehnelt, M.G., Kauffmann, G., 2000, *MNRAS*, 318L, 35H
- Haehnelt, M.G., Natarajan, P., Rees, M.J., 1998, *MNRAS*, 300, 817H
- Heger et al., 2003, *ApJ*, 591, 288H
- Heggie, D.C., Hut, P., Mineshige, S., Makino, J., Baumgardt, H., 2007, *PGASJ*, 59L, 11H
- Hernquist, L., 1989, *Natur*, 340, 687
- Herrmann, F., Hinder, I., Shoemaker, D., Laguna, P., Matzner, R.A., 2007, *ApJ*, 661, 430H
- Ho, L., 2008, *astro-ph/0803.2268*
- Holley-Bockelmann, K., & Richstone, D.O., 1999, *ApJ*, 517, 92H
- Holley-Bockelmann, K., & Sigurdsson, S., 2006, *astro-ph*, 1520H
- Holley-Bockelmann, K., Gultekin, K., Shoemaker, D., & Yunes, N. 2007, *ArXiv e-prints*, 707, *arXiv:0707.1334*
- Holley-Bockelmann, K., Micic, M., Sigurdsson, S., Rubbo, L., 2010, *ApJ*, 713, 1016
- Hopkins, P.F., Hernquist, L., Cox, T.J., Di Matteo, T., Martini, P., Robertson, B., Springel, V., 2005, *ApJ*, 630, 705H
- Hopkins, P. F., Hernquist, L., Cox, T. J., Robertson, B., Krause, E., 2007, *ApJ*, 669, 67H
- Hopkins, P. F., Hernquist, L., 2009, *ApJ*, 698, 1550H
- Hopkins, P. F., Murray, N., Quataert, E., Thompson, T. A., 2010, *MNRAS*, 401L, 19H
- Hu, J., Shen, Y., Lou, Y., Zhang, S., 2006, *ApJ*, 365, 345
- Islam, R. R., Taylor, J. E., Silk, J., 2003, *MNRAS*, 340, 647I
- Islam, R. R., Taylor, J. E., Silk, J., 2004, *MNRAS*, 354, 427I
- Kauffmann, G., Haehnelt, M., 2000, *MNRAS*, 311, 576K
- Kazantzidis, S., Mayer, L., Colpi, M., Madau, P., Debatista, V.P., Wadsley, J., Stadel, J., Quinn, T., Moore, B., 2005, *ApJ*, 623L, 67K
- Keres, D., Katz, N., Weinberg, D.H., Dave, R., 2005, *MNRAS*, 363, 2
- Kesden, M., Sperhake, U., Berti, E., 2010, *ApJ*, 715, 1006K
- Komossa, S., Zhou, H., Lu, H., 2008, *ApJ*, 678L, 81K
- Koppitz, M., Pollney, D., Reisswig, C., Rezzolla, L., Thornburg, J., Diener, P., Schnetter, E., 2007, *gr.qc*, 1163K
- Kormendy, J., Richstone, D., 1995, *ARA&A*, 33, 581K
- Koushiappas, S.M., Bullock, J.S., Dekel, A., 2004, *MNRAS*, 354, 292K
- Kravtsov, A.V., Gnedin, O.Y., Klypin, A.A., 2004, *ApJ*, 609, 482K
- Lehner, L., Moreschi, O.M., 2007, *PhRvD*, 7614040L
- Loeb, A., Rasio, F.A., 1994, *ApJ*, 432, 52L
- Lousto, C.O., Zlochower, Y., 2009, *PhRvD*, 79f4018L
- Maccarone, T.J., 2004, *MNRAS*, 35, 1049M
- Maccarone, T.J., Fender, R.P., Tzioumis, A.K., 2005, *MNRAS*, 356, L17
- Maccarone, T.J., 2005, *MNRAS*, 360, L30
- Mack, K.J., Ostriker, J.P., Ricotti, M., 2007, *ApJ*, 665, 1277M
- Madau, P., Rees, M.J., 2001, *ApJ*, 551L, 27M
- Makino, J., 1997, *ApJ*, 478, 58M
- Marconi, A., Hunt, L. K., 2003, *ApJ*, 589, L21
- Marconi, A., Risaliti, G., Gilli, R., Hunt, L.K., Maiolino, R., Salvati, M., 2004, *MNRAS*, 351, 169
- Matthews, W.G., Brighenti, F., 2003, *ApJ*, 599, 992M
- Mayer, L., Kazantzidis, S., Madau, P., Colpi, M., Quinn, T., Wadsley, J., 2007, *Sci*, 316, 1874M
- McWilliams, S.T., 2008, *PhDT*, 7M
- Melia, F., Falcke, H., 2001, *ARA&A*, 39, 309M
- Menou, K., Haiman, Z., Narayanan, V.K., 2001, *ApJ*, 558, 535
- Merloni, A., 2004, *MNRAS*, 353, 1035
- Merritt, D., Ferrarese, L., Joseph, C. L., 2001, *Science*, 293, 1116M
- Merritt, D., Milosavljevic, M., Favata, M., Hughes, S.A., Holz, D.E., 2004, *ApJ*, 607L, 9M
- Mihos, J.C., Hernquist, L., 1994, *ApJ*, 425L, 13M
- Miller, M.C., Colbert, E.J.M., 2004, *IJMPD*, 13, 1M
- Milosavljevic, M., Merritt, D., 2001, *ApJ*, 563, 34M
- Milosavljevic, M., Merritt, D., 2003, *ApJ*, 596, 860M

- Micic, M., Abel, T., Sigurdsson, S., 2006, MNRAS, 372, 1540M
- Micic, M., Holley-Bockelmann, K., Sigurdsson, S., Abel, T., 2007, MNRAS, 380, 1533M
- Monaco, P., Salucci, P., Danese, L., 2000, MNRAS, 311, 279M
- Navarro, J.F., Frenk, C.S., White, S.D.M., 1995, ApJ, 462, 563N
- Nayakshin, S., Wilkinson, M. I., King, A., 2009, MNRAS, 398, 54N
- Ostriker, J.P., Choi, E., Ciotti, L., Novak, G.S., Proga, D., 2010, ArXiv e-prints, 1004, arXiv:1004.2923
- O'Sullivan, E., Forbes, D.A., Pnman, T.J., 2001, MNRAS, 328, 461O
- Pedersen, K., Rasmussen, J., Sommer-Larsen, J., Toft, S., Benson, A.J., Bower, R.G., 2006, NewA, 11, 465P
- Portegies Zwart, S.F., Baumgardt, H., Hut, P., Makino, J., McMillan, S.L.W., 2004, Natur, 428, 724P
- Quataert, E., Gruzinov, A., 2000, ApJ, 545, 842Q
- Quinlan, G.D., 1996, NewA, 1, 35Q
- Rees, M.J., 1984, ARA&A, 22, 471R
- Richstone, D.O., 1976, ApJ, 204, 642
- Robertson, B., Hernquist, L., Cox, T.J., Di Matteo, T., Hopkins, P.F., Martini, P., Springel, V., 2006, ApJ, 641, 90R
- Sales, L.V., Navarro, J.F., Abadi, M.G., Steinmetz, M., 2007, MNRAS, 379, 1464
- Schneider, R., Ferrara, A., Natarajan, P., Omukai, K., 2002, ApJ, 571, 30S
- Schnittman, J.D., 2007, ApJ, 667L, 133S
- Schnittman, J.D., Buonanno, A., 2007, ApJ, 662L, 63S
- Sesana, A., 2007, MNRAS, 382L, 6S
- Shakura, N.I., Syunyaev, R.A., 1973, A&A, 24, 337S
- Shankar, F., Lapi, A., Salucci, P., De Zotti, G., Danese, L., 2006, ApJ, 643, 14S
- Sigurdsson, S., 2003, CQGra, 20S, 45S
- Sijacki, D., Springel, V., di Matteo, T., Hernquist, L., 2007, MNRAS, 380, 877S
- Sijacki, D., Springel, V., Haehnelt, M.G., 2009, MNRAS, 400, 100S
- Silk, J., Rees, M.J., 1998, A&A, 331L, 1S
- Sinha, M., Holley-Bockelmann, K., 2010, MNRAS, 405L, 31S
- Soltan A., 1982, MNRAS, 200, 115S
- Somerville, R., Hopkins, P.F., Cox, T.J., Robertson, B.E., Hernquist, L., 2008, MNRAS, 391, 481S
- Sperhake, U., 2009, LNP, 769, 125S
- Taffoni, G., Mayer, L., Colpi, M., Governato, F., 2003, MNRAS, 341, 434T
- Tremaine, S., et al. 2002, ApJ, 574, 740T
- Trenti, M., Stiavelli, M., 2009, ApJ, 694, 879T
- Trenti, M., Stiavelli, M., Michael S. J., 2009, ApJ, 700, 1672L
- Valluri, M., Ferrarese, L., Merritt, D., Joseph, C. L. 2005, ApJ, 628, 137
- van der Marel, R.P., 2004, cbhg.symp, 37V
- Volonteri, M., Haardt, F., Madau, P., 2003, ApJ, 582, 559
- Volonteri, M., 2007, ApJ, 663L, 5V
- Volonteri, M., Gultekin, K., Dotti, M., 2010, astro-ph/1001.1743
- Weinberg, M.D., 1989, MNRAS, 239, 549
- Wise, J., H., Abel, T., 2005, ApJ, 629, 615W
- Wyithe, J.S.B., Loeb, A., 2005, ApJ, 634, 910W